2020

FGGY Carbohydrate Kinase Domain Containing is Induced During Skeletal Muscle Atrophy and Modulates Map Kinase and AKT Signaling

Anastasia L. Smith
University of North Florida, anastasiasmith1221@gmail.com

FGGY CARBOHYDRATE KINASE DOMAIN CONTAINING IS INDUCED DURING SKELETAL MUSCLE ATROPHY AND MODULATES MAP KINASE AND AKT SIGNALING

By

Anastasia Lisa Smith

A thesis submitted to the Department of Biology

in partial fulfillment of the requirements for the degree of

Master of Science in Biology

UNIVERSITY OF NORTH FLORIDA

COLLEGE OF ARTS AND SCIENCES

December, 2020

CERTIFICATE OF APPROVAL

The thesis “Fggy Carbohydrate Kinase Domain Containing is Induced During Skeletal Muscle Atrophy and Modulates MAP Kinase and AKT Signaling” submitted by Anastasia Smith

Approved by the thesis committee: Date

_____ _____
Dr. David Waddell, Ph.D.
Committee Chairperson

_____ _____
Dr. Frank Smith, Ph.D.

_____ _____
Dr. Wolfdieter Springer, Ph.D.

Table of Contents

List of Figures

List of Tables

Abstract

Skeletal muscle atrophy can result from a range of physiological conditions, including denervation, immobilization, hindlimb unweighting, and aging. To better characterize the molecular genetic events of atrophy, a microarray was performed using skeletal muscle isolated from mice after 3 and 14 days of denervation and compared to control muscle to identify novel atrophy-induced genes. The microarray revealed that FGGY carbohydrate kinase domain containing (Fggy) is expressed in skeletal muscle and is induced in response to denervation. Bioinformatic analysis of the Fggy gene locus revealed two validated alternative isoforms, that we have termed Fggy-L-552 and Fggy-S-387, which have distinct transcription initiation sites. In order to confirm that Fggy is expressed in muscle, the cDNAs of the two validated alternative variants were cloned from myoblast cells. Interestingly, two novel alternative splice variants, designated Fggy-L-482 and Fggy-S-344, were also cloned, suggesting that at least four Fggy splice variants are expressed in skeletal muscle. Quantitative RT-PCR (RT-qPCR) was performed using RNA isolated from muscle cells and primers designed to distinguish the four alternative Fggy transcripts. The RT-qPCR data reveals that the Fggy-L transcripts are more highly expressed during myoblast differentiation, while the Fggy-S transcripts show relatively stable expression in proliferating myoblasts and differentiated myotubes. Confocal fluorescent microscopy revealed that the Fggy-L variants appear to localize evenly throughout the cytoplasm, while the Fggy-S variants produce a more punctuate localization pattern throughout the cytoplasm of proliferating muscle cells. Finally, ectopic expression of Fggy-L-552 and Fggy-S-387 resulted in inhibition of muscle cell differentiation and attenuation of the MAP kinase and AKT signaling pathways. The characterization of novel genes induced during neurogenic atrophy helps improve our understanding of the molecular and cellular events that lead to muscle atrophy and may eventually lead to new therapeutic targets for the treatment of muscle wasting.

Chapter 1: Skeletal Muscle Atrophy, MuRF1, and Muscle Cell Signaling

Skeletal Muscle Atrophy

Skeletal muscle atrophy is a decrease in the total muscle mass due to the rate of protein degradation outpacing the rate of protein synthesis (Bodine and Baehr, 2014). This change can be caused by a variety of physiological conditions, including aging, neuronal injury, disuse, and corticosteroid treatment (Bodine and Baehr, 2014). Atrophy is not specific to one disease, has many levels of severity, and is multifactorial, suggesting there may not be one simple way to prevent muscle wasting. However, having clearer insight into how the body regulates muscle atrophy may provide important information for the identification and development of new therapeutic targets to prevent this process.

MuRF1 and MAFbx

To explore atrophy at the molecular level, a study using rats undergoing muscle atrophy identified two E3 ubiquitin ligases named Muscle RING Finger 1 (MuRF1) and Muscle Atrophy F-Box (MAFbx) as being upregulated in virtually all atrophy models, including denervation, immobilization, unweighing, and treatment with interleukin-1 (IL-1) or dexamethasone (Bodine et al, 2001). A number of genes were observed to have differential expression under one or two conditions but only MuRF1 and MAFbx were found to be upregulated under all conditions (Fig. 1). This study also showed that MuRF1 and MAFbx null mice are resistant to skeletal muscle atrophy (Bodine et al, 2001). After transection of the sciatic nerve, MuRF1 knockout mice showed 36% muscle sparing at 14 days of denervation, while MAFbx knockout mice showed 56% sparing

at 14 days post denervation (Bodine et al, 2001). These findings demonstrated that MuRF1 and MAFbx are likely involved in a common atrophy cascade. Moreover, MuRF1 and MAFbx are known E3 ubiquitin ligases, and believed to participate in muscle atrophy by targeting substrate proteins for degradation via the ubiquitin proteasome pathway.

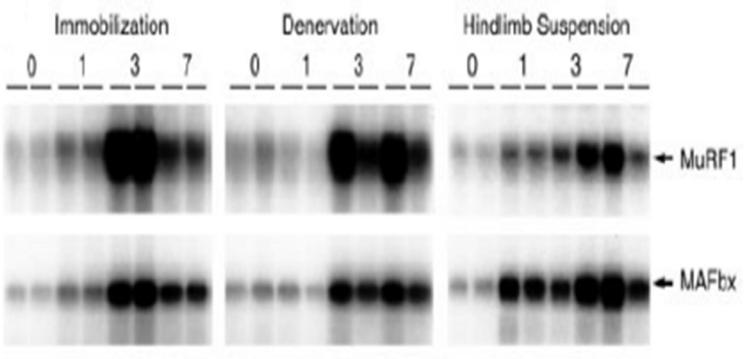

Figure 1. **MuRF1 and MAFbx are upregulated during muscle atrophy.** Northern blot analysis of MuRF1 and MAFbx in muscle isolated from rats subjected to atrophy induction by immobilization, denervation, and hind limb suspension. Increased expression of MuRF1 and MAFbx was observed at day 1 and reached a peak at day 3 post-denervation (Bodine et al, 2001).

The Ubiquitin Proteasome System

Ubiquitin is a small, abundant protein that covalently attaches to target proteins, which frequently leads to degradation by the 26S proteasome (Borlepawar et al, 2018). Prior to attachment to target proteins, ubiquitin must first be activated by an E1 ubiquitin activating enzyme. The activated ubiquitin then binds to an E2 ubiquitin conjugating enzyme, which transfers the ubiquitin to the targeted protein with the E3 ligating enzyme serving as a platform to bring the E2 and substrate protein into proximity (Fig. 2). Protein degradation via the Ubiquitin Proteasome System (UPS) is very specific and although there are only two E1 enzymes (Jin et al., 2007) and about 40 E2 enzymes (Stewart et al., 2016), there are around 600 different E3 enzymes that provide substrate specificity and allow this system to act in a precise manner (Mearini et al., 2008). UPS activity has been characterized under multiple physiological conditions that lead to muscle loss, including

denervation (Medina, Wing, and Goldberg, 1995), disuse (Taillander et al, 1996), and cancer cachexia (Temparis et al, 1994;Baracos, 1995).

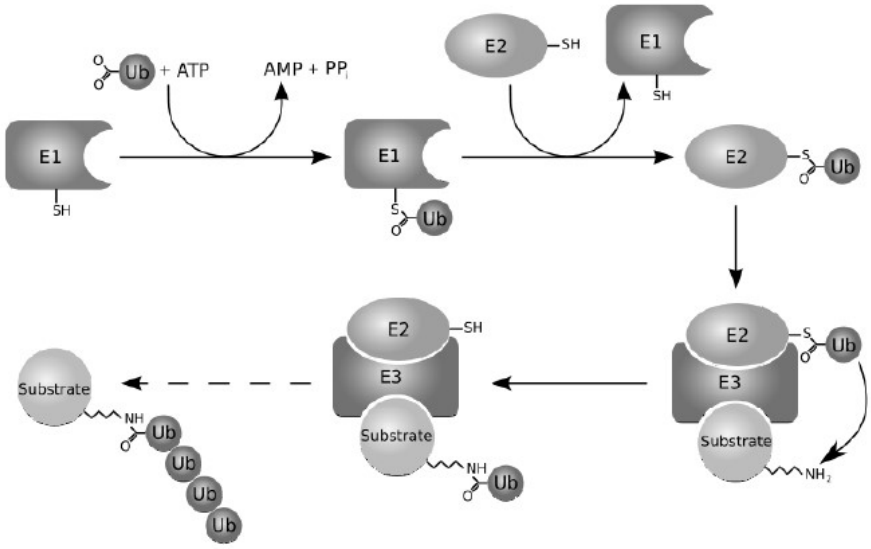

Figure 2. Schematic of the ubiquitin proteasome system. The E1 ubiquitin activating enzyme, E2 ubiquitin conjugating enzyme, and E3 ubiquitin ligase form a pathway to ubiquitinate substrates for degradation by the 26s proteasome (Dodd, 2011).

MuRF1 as a Putative Transcriptional Regulator

MuRF1 is a member of the tripartite motif (TRIM) family of E3 ubiquitin ligases that are characterized by a RING domain, a zinc-finger B-box domain, and a leucine-rich coiled-coil domain (Bodine and Baehr, 2014). The RING domain of E3 ubiquitin ligases functions by bringing substrate proteins and activated ubiquitin from the E2 into direct contact. The RING domain is believed to perform the catalytic activity of MuRF1, while the zinc-finger B-box domain is suggested to function in binding to target proteins (Ikeda et al, 2013).

Although there are many studies focusing on its role in the UPS, there are other studies indicating MuRF1 may have an additional role as a transcriptional modulator (Furlow et al, 2013). One study suggests that MuRF1 may serve as a negative transcriptional regulator of itself and of MAFbx, but

it is unclear if this regulation is direct or indirect (Furlow et al, 2013). To investigate MuRF1 further, a MuRF1 knockout mouse was created by inserting a β-galactosidase lacZ cassette into the MuRF1 locus, putting the β-galactosidase gene under the control of the endogenous MuRF1 promoter and creating a MuRF1 reporter gene within the mouse genome (Bodine et al, 2001). When analyzing MuRF1 expression in denervated muscles from wild type mice, it was found that MuRF1 levels increase by 3 days of denervation but return to baseline by 14 days of denervation (Furlow et al, 2013). In contrast, MuRF1 gene locus activity does not return to baseline in the MuRF1-null mice as measured by β-galactosidase expression in the KO mice, suggesting that lack of MuRF1 leads to a failure to inhibit the MuRF1 promoter (Fig. 3A-B). Furthermore, this same study also showed that mice lacking MuRF1 failed to down regulate MAFbx expression after 14 days of denervation (Fig. 3C-D). Finally, the microarray study revealed that MuRF1 KO leads to differential expression of a number of other genes in response to denervation including a gene named Fggy Carbohydrate Kinase Domain Containing (Fggy) (Furlow et al, 2013).

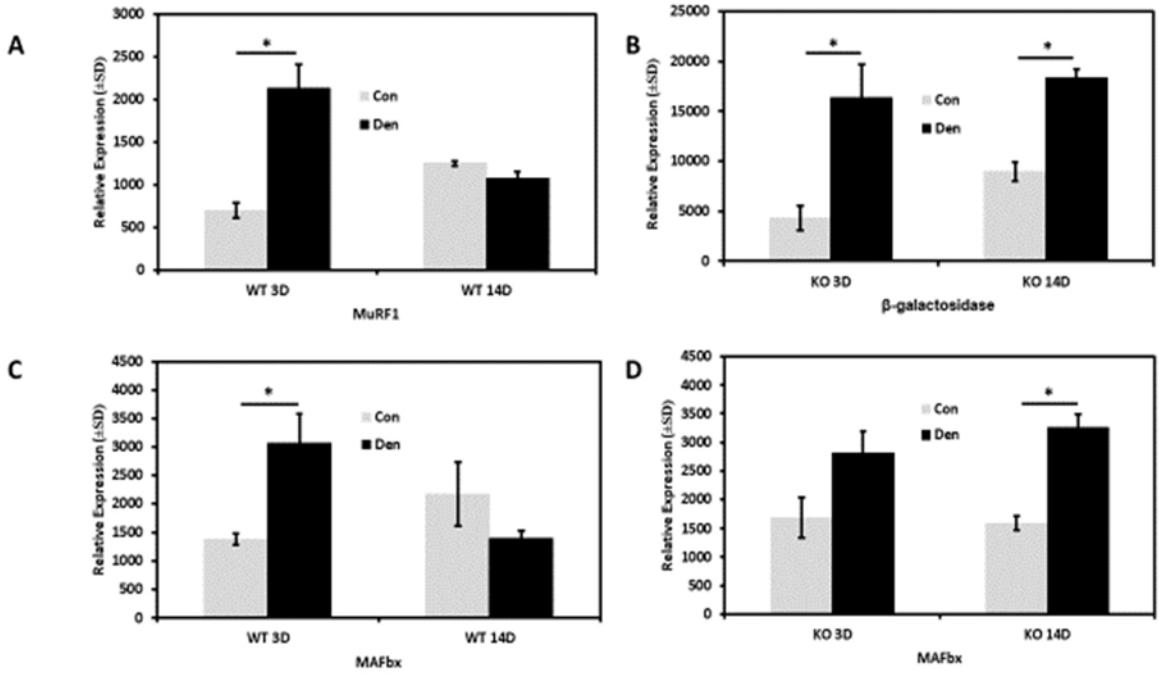

Figure 3. Transcriptional activity of the MuRF1 gene locus and MAFbx in WT and MuRF1 KO mice post-denervation. (A) Denervated WT mice show an increase in MuRF1 gene expression at day 3 (3D) but returns to baseline at day 14 (14D) post-denervation. (B) Denervated KO mice show an increase in β-galactosidase expression, which is under the control of the MuRF1 promoter, at day 3 and expression remained elevated at day 14 post-denervation. (C) Denervated WT mice show an increase in MAFbx gene expression at day 3 (3D) but a return to baseline levels by day 14 (14D) post-denervation. (D) Denervated MuRF1 KO mice showed increased expression in MAFbx at day 3 (3D) that remained elevated at day 14 (14D) (Furlow et al, 2013).

Mitogen-activated protein kinase signaling

MAPK signaling is essential for the expression of muscle specific genes, muscle growth, and differentiation of muscle cells (Fig. 4) (Bennett and Tonks, 1997). It has previously been shown that MAPK signaling is critical for muscle cell differentiation, specifically complete differentiation and fusion of myoblasts into myotubes (Bennett and Tonks, 1997). The four branches of the MAP kinase signaling pathway include extracellular signal-regulated kinases 1 and 2 (ERK1/2), c-Jun amino-terminal kinase (JNK), p38, and ERK5 (Bennett et al, 1997). Moreover, the ERK1/2 branch has been linked to the regulation of skeletal muscle cell growth and differentiation (Bennett and Tonks, 1997). Specifically, the inactivation of this branch has been found to promote myogenesis

initiation (Adi et al, 2002; Bennett and Tonks, 1997) by leading to the upregulation of differentiation factors specific to skeletal muscle cell differentiation, including myogenin (Penna et al, 2010). Previous work from our lab has identified a number of genes that are differentially expressed in the MuRF1 KO model in response to denervation that are also linked to MAPK signaling. For example, Dual-specificity phosphatase 29 (Dusp29) and Dual-specificity phosphatase 4 (Dusp4), which are part of a large group of phosphatases that regulate the MAPK pathway (Caunt et al., 2012), have been shown to decrease the activity of the ERK1/2 branch (Cooper et al., 2020; Haddock et al., 2019). Further, Tetratricopeptide repeat domain containing 39C (Ttc39c) and Family with sequence similarity 83 Member D (Fam83D), which are two putative scaffolding proteins important for modulating proper muscle cell signaling pathways, including the ERK1/2 branch of the MAP kinase signaling cascade, have been found to be differentially regulated in MuRF1 KO mice following denervation (Hayes et al., 2019; Cooper et al., 2020). Additionally, protein phosphatase methylesterase (Ppme1) has been found to regulate the MAPK signaling pathway through the ERK1/2 branch of MAP kinase signaling and inhibition of Ppme1 led to a decrease in whole ERK1/2 expression, as well as ERK1/2 phosphorylation levels (Labuzan et al., 2020).

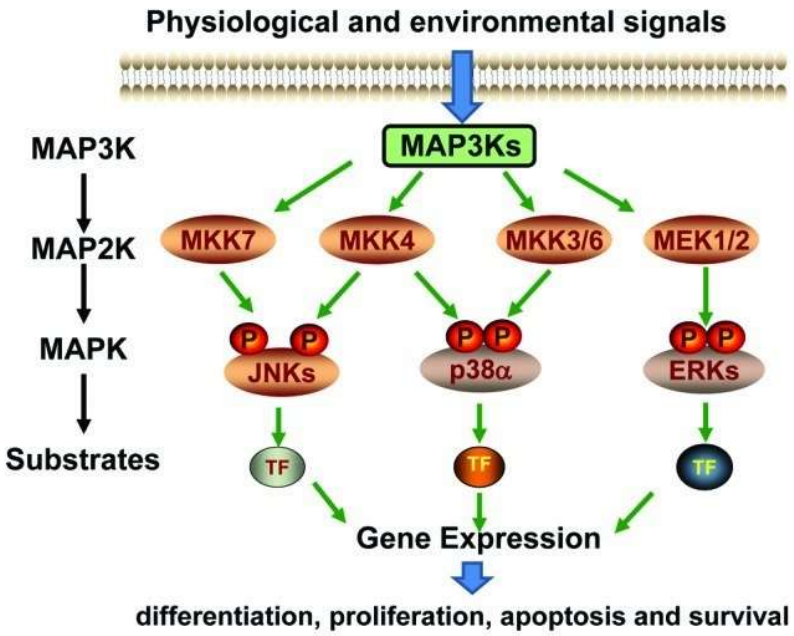

Figure 4. Schematic of the MAPK signaling pathways (Wang, Xia, 2012).

AKT signaling cascade

In addition to MAPK signaling, AKT signaling is also known to be involved in the modulation of skeletal muscle mass (Hitachi and Tsuchida, 2014). The upstream regulator of AKT and mTOR, insulin-like growth factor-1 (IGF-1), is responsible in part for the induction of protein synthesis (Fig. 5) (Hitachi and Tsuchida, 2014). IGF-1 inhibits muscle atrophy and promotes muscle hypertrophy by activation of the AKT signaling pathway, which is known to promote protein synthesis in three ways; 1) by inhibition of GSK-3β, 2) by inhibition of the FoxO family of transcription factors, and 3) by activation of the mTOR pathway (Hitachi and Tsuchida, 2014). Glycogen synthase kinase 3 β (GSK-3β) is constitutively active and functions by inhibiting protein synthesis (MacAulay and Woodgett, 2008). Activated AKT phosphorylates GSK-3β to inactivate it, which allows its target proteins to become dephosphorylated (MacAulay and Woodgett, 2008). Forkhead box O (FoxO) is a family of transcription factors that activate the transcription of MuRF1

and MAFbx and promote muscle atrophy (Sandri et al., 2004). AKT phosphorylation of FoxO transcription factors inhibits their translocation into the nucleus and ability to activate atrophy promoting genes (Sandri et al., 2004). The activation of mTOR by AKT allows it to phosphorylate 4E-BP1 which prevents it from binding and inactivating the initiation factor eIF4E, which leads to the release of eIF4E and a concomitant increase in protein translation levels within the muscle cell (Alessi et al., 1996; Tsai et al., 2015). Overall, the activation of the AKT signaling cascade results in a decrease in protein degradation via FoxO inactivation and an attenuation of MuRF1 and MAFbx activation. Moreover, AKT activation also leads to an increase in protein synthesis via GSK-3β inhibition and mTOR activation, which promotes muscle hypertrophy.

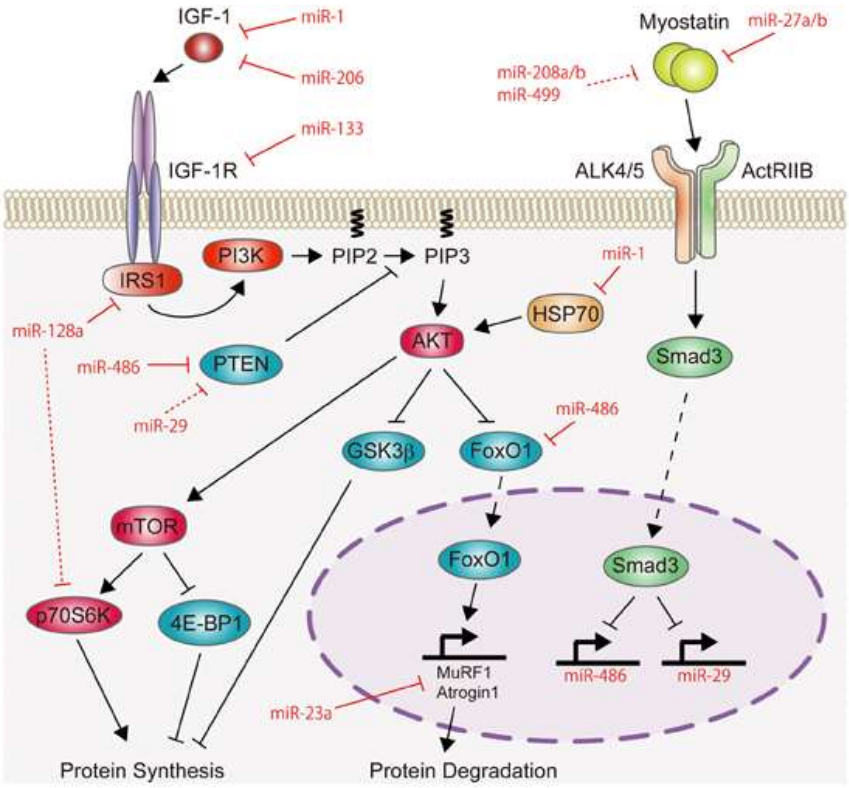

Figure 5. Schematic of the AKT signaling pathway in skeletal muscle (Hitachi and Tsuchida, 2014).

Chapter 2: Identification and characterization of Fggy carbohydrate kinase domain containing in skeletal muscle

Introduction

The FGGY Carbohydrate Kinase Family

The Fggy gene belongs to an evolutionarily related family of carbohydrate kinases that have been found to phosphorylate an array of various sugar substrates (Zhang et al., 2011). The Fggy carbohydrate kinase family includes, L-fucolokinase, gluconokinase, glycerol kinase, D-ribulose kinase, and L-xylulose kinase (Omelchenko et al., 2010). Of these, the glycerol kinases are the most widely conserved between the three domains of life (Fig. 6).

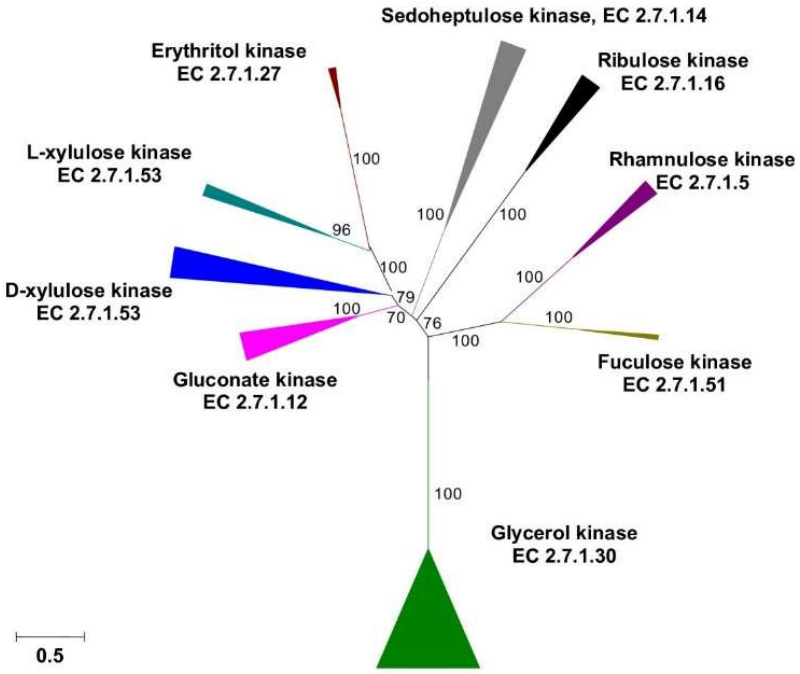

Figure 6. Phylogenetic tree of the Carbohydrate kinases of the FGGY family (Omelchenko et al., 2010).

The FGGY kinase family also consists of a subgroup, similar to the xylulose kinase, that phosphorylates autoinducer-2 (AI-2). AI-2 is a bacterial signaling molecule that plays a role in regulating bacterial behaviors such as cell to cell communication, biofilm formation, and gene expression (Xavier et al., 2007; Vendeville et al., 2005). Additionally, the rate of AI-2 synthesis and uptake has been shown to be elevated in the presence of glucose (Wang et al., 2005). Although characterization of the functional role of this diverse family of kinases remains ongoing, it is known that they possess two conserved domains referred to as the N-terminal (FGGY-N) and C-terminal (FGGY-C) (Hurley et al., 1996; Hurley et al., 1993). The two domains both adopt a ribonuclease H-like fold and the cleft formed between the two domains acts as the binding site for substrates, as well as ATP (Hurley et al., 1993).

Fggy carbohydrate kinase domain-containing

The Fggy carbohydrate kinase domain-containing gene (Fggy) encodes a protein with at least 90% conservation between humans, mice, and rats (Madiera et al., 2019). In humans, it is found on the short arm of the first chromosome and in mice it is found on the fourth chromosome.

A previous study in HEK293 cells found that Fggy may function in the pentose phosphate pathway (also known as the phosphogluconate pathway or hexose monophosphate shunt) and is a metabolic pathway that runs parallel to glycolysis, but appears to play a primary role in the generation of precursors for the synthesis of nucleotides (Fig. 7) (Singh et al., 2017; Ge et al., 2020). Fggy has previously been suggested to be associated with sporadic amyotrophic lateral sclerosis (S-ALS) (Dunckley et al., 2007), but further studies have failed to corroborate these results which might be due to the complexity of this multifactorial disease (Doud et al., 2012 and Cai et al., 2014). Although previous studies have not generated a consensus regarding a role for Fggy in S-ALS

development of progression, it is an intriguing possibility since we identified Fggy as a novel neurogenic atrophy-induced gene in skeletal muscle.

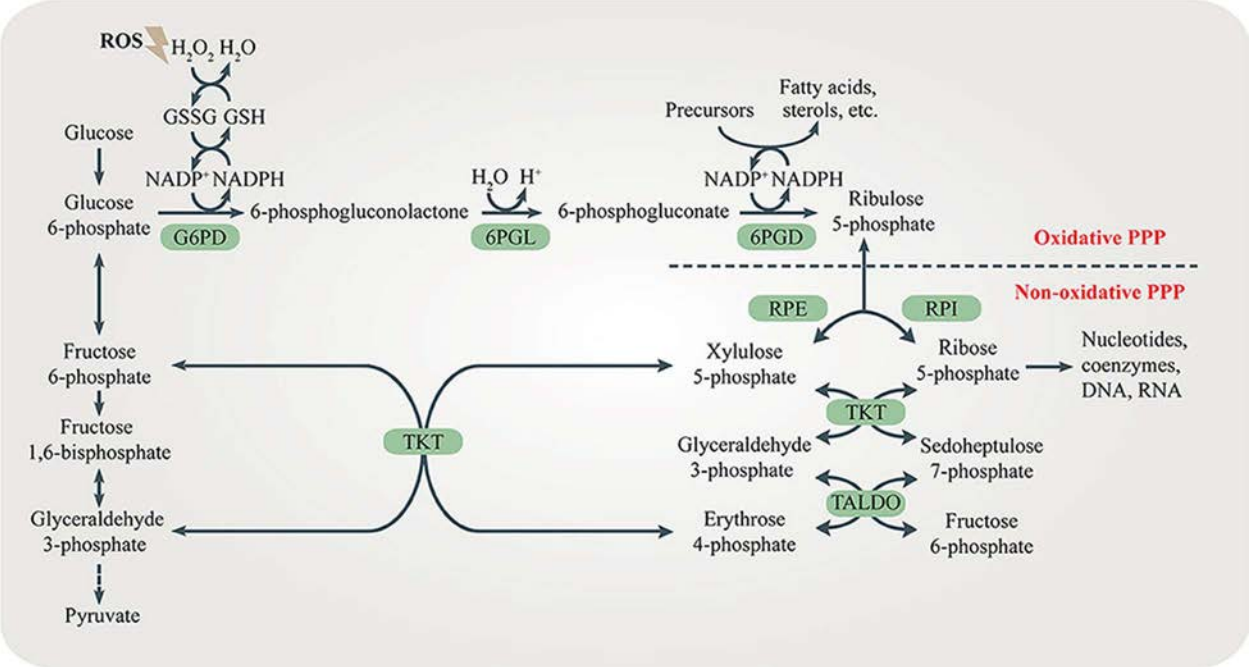

Figure 7. Schematic of the pentose phosphate pathway (PPP). Enzymes in the oxidative and non-oxidative PPP are shaded in green (Ge et al., 2020).

In addition to a putative role in skeletal muscle, Fggy has also been identified as a tumor suppressor gene and as a potential biomarker for the severity of lung squamous cell carcinoma (LUSC) due to an observed negative relationship between the expression of a Fggy mutant isoform and LUSC prognosis (Zhang et al., 2019). Specifically, poor LUSC clinical outcomes have been linked to a specific mutant variant of the Fggy gene designated LINE-1-FGGY (L1-FGGY). L1-FGGY is generated when a transposon, called the long-interspersed element 1 (LINE-1), is inserted into the beginning of the thirteenth exon of Fggy via retro-transposition which inactivates the Fggy gene (Zhang et al 2019). Inactivation of the Fggy gene resulted in increased cell proliferation and dysregulation of cell energy metabolism further suggesting a role of Fggy in energy metabolism and identifying a new role for Fggy in regulating cell proliferation (Zhang et al 2019). Finally, in

adipose tissue, a low dose of bisphenol A (BPA) exposure in fetal mice decreased the instance of hypermethylation of the Fggy promoter which lead to an increase in Fggy transcription (Taylor et al., 2018). As a result, an increase in the amount of adipose tissue and diet induced obesity in adult mice was observed (Taylor et al., 2018). Previous studies linking Fggy to cell metabolism, adipose tissue development, and regulation of cell proliferation provide intriguing insights into the potential functional role that Fggy may play in the molecular mechanisms of skeletal muscle atrophy. Here, we present the first investigation of the role that Fggy plays in skeletal muscle.

Materials and Methods

Animals

There were no animal experiments related to the current study conducted at the University of North Florida; however, the sex, age range, strain, and treatment conditions of the animals used for the Illumina array studies, as well as the IUCAC approvals, have been previously described (Furlow et al., 2013)

Cell Culture

C_2C_{12} mouse myoblasts were maintained in Dulbecco's Modified Eagle's Medium (DMEM) (Thermo Fischer Scientific, Waltham, MA) supplemented with 1X Penicillin/Streptomycin and Gentamicin (Thermo Fischer Scientific, Waltham, MA), non-essential amino acids (GE Healthcare HyClone Laboratories, Logan, UT), and 10% Fetal Bovine Serum (FBS) (GE Healthcare HyClone Laboratories, Logan, UT). Cells were grown in a humidified chamber at 37° C and 5% CO_2. DMEM with 2% FBS, Penicillin/Streptomycin and Gentamicin, and non-essential amino acids was used to induce C_2C_{12} myoblast differentiation when cells reached 100% confluency.

RNA isolation and complementary DNA synthesis

Total RNA was isolated from C_2C_{12} cells using the RNeasy Mini Kit (Qiagen, Valencia, CA) and following the manufacturer's instructions. Isolated RNA was used to synthesize complementary DNA (cDNA) using a PolyT primer and Moloney Murine Leukemia Virus (M-MLV) Reverse Transcriptase (Thermo Fisher Scientific, Waltham, MA) and following the manufacturer's instructions.

Cloning of the Fggy cDNA

Gene specific primers (Table 1) were designed using the gene sequences for murine Fggy-L (GenBank accession number: NM_001113412.1) and Fggy-S (GenBank accession number: NM_029347.2) and mixed with template DNA generated by reverse transcription as described above, and Taq polymerase. PCR reactions were performed by following the manufacturer's protocol (Life Technologies, Grand Island, NY).

Fggy open reading frames (ORFs) were cloned into the pGEM-T Easy vector using the manufacturer's provided protocol (Promega, Madison, WI) and sequenced to confirm the absence of mutations using the Big Dye Sanger terminator sequencing method (Eurofins MWG Operon, Huntsville, AL). Fggy ORFs were sub-cloned into the HindIII and BamHI restriction sites of the pcDNA3.1 1(+) (ThermoFisher Scientific, Waltham, MA) and pEGFP-C3 (Clontech, Mountain View, CA) expression plasmids and sequenced to confirm correct orientation.

Table 1. Primer Sequences (5' to 3')

Primer Name	**Sequence**
Fggy-cDNA3-L-552-F	GCAAGCTTACCATGATGTCTGGCAGAGACCAGG
Fggy-cDNA3- L-552-R	GCGGATCCGGACAGGTATGTTCAGCTTCCATTCATG
Fggy-cDNA3-S-387-F	GCAAGCTTACCATGATGTCTGGCAGAGACCAGG
Fggy-cDNA3- S-387-R	GCGGATCCGCATTCTTAAAATGCTTTAGAAGAAG
Fggy-L-482-qPCR-F	AGATCCAGTGTTTGTACCAGG
Fggy-L-482-qPCR-R	CCAGTGACCAATTTTCCAGTC
Fggy- L-552-qPCR-F	ATGGCAACCGGTCTCCCTTAG
Fggy- L-552-qPCR-R	TTGAACAGTGGCCAGGTAGAG
Fggy-S-344-qPCR-F	GCAAAATAGGAGTGATTGGGG
Fggy-S-344-qPCR-R	CACTGGATCTTTGCTGATCCC
Fggy- S-387-qPCR-F	ATCGTCCCTGGGTTCTGGTTG
Fggy- S-387-qPCR-R	CTGTAGGTTTCTGGCTGTGGC

Reporter Assays

Mouse myoblasts were plated in 12-well dishes at approximately 75,000 cells/well and allowed to proliferate overnight prior to transfection. Transfections were performed at 70-80% confluence using Turbofect Transfection Reagent (Thermo Scientific, Rockford, IL) and following the manufacturer's protocol. Cells were overlaid with 1 μg per well of total DNA, including 250 ng/well of reporter plasmid, 125 ng/well of β -galactosidase (β-gal) as an internal control, and

empty pBluescript plasmid to a final concentration of 1 μg/well. The DNA had been allowed to complex with the transfection reagent for 20 minutes prior to cell overlay. After 24 hours, culture media was changed from 10% to 2% serum to induce differentiation. Media was harvested at 48 h, 96 h, and 144 h post-media change to analyze secreted embryonic alkaline phosphatase (SEAP) levels. The Phospha-Light SEAP Reporter Gene Assay Kit (Life Technologies, Grand Island, NY) was used per the manufacturer's instructions protocol to detect SEAP levels using a Biotec Synergy 2 microplate reader set for an endpoint read with a 2 s integration time to assess levels of luminescence. To adjust for variations in transfection efficiency between wells, β -gal activity was analyzed. Cells were lysed with Passive Lysis Buffer (Promega, Madison, WI) and homogenates cleared by centrifugation. Cell lysates were incubated with ortho-nitrophenyl-β-D-galactopyranoside (ONPG) dissolved in Z Buffer (60 mM Na2HPO4·7H2O, 40 mM NaH2PO4·H2O, 10 mM KCl, 1 mM MgSO4, 50 mM β-mercaptoethanol, pH 7.0) overnight at 37 °C. SEAP activity was divided by the β -gal activity to achieve corrected SEAP values.

Reverse transcription quantitative PCR

Reverse transcription quantitative PCR (RT-qPCR) was carried out using total RNA isolated from C_2C_{12} cells and the iScript cDNA Synthesis Kit according to the manufacturer's protocol (Bio-Rad, Hercules, CA). The reverse transcription of isolated RNA yielded complementary DNA (cDNA) that was then used for analysis of Fggy gene expression in C_2C_{12} cells. Gene specific primers (Table 1) cDNA, and iTaq Universal SYBR Green Reaction Supermix were mixed according to the manufacturer's instructions (Bio-Rad, Hercules, CA) and analyzed on the CFX Connect Real-Time PCR Detection System (Bio-Rad, Hercules, CA). The experiment was repeated as least two times and each condition was performed in biological triplicate, each individual biological replicate was used for cDNA amplification in duplicate, and each cDNA

amplification replicate was done in technical triplicates (three biological replicates × two cDNA synthesis replicates × three technical replicates = 18 individual reads per biological sample). The Fggy expression data was calculated after normalization to GAPDH expression using the $2^{-\Delta\Delta Ct}$ method.

Protein purification and Western blot analysis

Protein purification was achieved as previously described (Haddock et al., 2019, Hayes et al., 2019, Lynch et al., 2019). Briefly, mouse myoblasts were cultured in 10 cm plates, harvested at various timepoints, and lysed for protein isolation. Fggy was exogenously expressed by transfection of cells with pcDNA3.1-Fggy expression plasmids after 24 hours of cell growth in 10% FBS media using Turbofect transfection reagent according to the manufacturer's instructions. Cells were then harvested at various timepoints of proliferation and differentiation and stored at −80 °C until cell lysis. Cells were lysed on ice in Universal Lysis Buffer (ULB)$^{(+)}$ (50 mM Tris, pH 7.5, 150 mM NaCl, 50 mM NaF, 0.5% NP-40, with addition of 1 mM PMSF, 1 mM DTT, 10 mM β-glycerophosphate, 2 mM sodium molbydate and a protease inhibitor cocktail), cleared by centrifugation, and total protein concentration was determined using the Quick Start Bradford 1X Dye Reagent and following the manufacturer's instructions (Bio-Rad, Hercules, CA).

Western blot procedures were conducted using 25-100 μg of protein run on a sodium dodecyl sulfate polyacrylamide gel electrophoresis (SDS PAGE) denaturing gel and transferred to polyvinylidene fluoride (PVDF) membrane (EMD Millipore, Billerica, MA). To verify the quality of the transfer and equal protein loading, the membranes were stained using Ponceau S prior to blocking the membrane in 5% dry milk dissolved in Tris-buffered saline and 0.05% Tween-20 (TTBS). The membranes were probed with anti-myosin heavy chain (MYH1/2/4/6), anti-myogenin, anti-p-ERK, anti-ERK, anti-AKT-phospho-S473, anti-AKT, anti-GAPDH, and anti-α

tubulin primary antibodies and subsequently probed with a corresponding HRP-conjugated secondary (Table 2). Westerns were developed by incubating the membrane with ECL Western Blotting Substrate (Thermo Fisher Scientific, Waltham, MA) and imaged using the Amersham Imager 600 RGB system (GE Healthcare Life Sciences, Marlborough, MA). For the use of multiple antibodies on a single blot, membranes were striped with a 10% SDS, 0.5 M Tris-HCl pH 6.8, β-mercaptoethanol solution, blocked again, and then probed and imaged as described previously. The intensity of the bands on the Western blots was quantified using the open access ImageJ software.

Table 2. List of antibodies used in this study

Antibody	**Source**	**Catalog #**	**Dilution**
anti-α-tubulin	Santa Cruz Biotechnology, Dallas, TX	sc-32293	WB: 1:1000
anti-Myosin Heavy Chain (MYH1/2/4/6)	Santa Cruz Biotechnology, Dallas, TX	sc-32732	WB: 1:1000
anti-myogenin	Santa Cruz Biotechnology, Dallas, TX	sc-12732	WB: 1:1000
anti-GAPDH	ProteinTech, Rosemont, IL	600041-lg	WB: 1:5000
anti-phospho-ERK	Santa Cruz Biotechnology, Dallas, TX	sc-7383	WB: 1:1000
anti-ERK	Santa Cruz Biotechnology, Dallas, TX	sc-94	WB: 1:1000
anti-Akt1-phospho-S473	ProteinTech, Rosemont, IL	66444-I-lg	WB: 1:2000
anti-Akt	ProteinTech, Rosemont, IL	602032-lg	WB: 1:5000
Mouse anti-rabbit IgG-HRP	Santa Cruz Biotechnology, Dallas, TX	sc-2357	WB: 1:5000
Rabbit anti-mouse IgG-HRP (H + L)	Thermo Scientific, Rockford, IL	PI31450	WB: 1:5000

Confocal fluorescent microscopy

Mouse myoblast cells were plated on 3.5 cm glass bottom plates at a seeding density of approximately 100,000 cells/plate and transfected with 2.5 μg of pEGFP-Fggy expression plasmids at 70-80% confluency. Cells were fixed at 48h post-plating with 4% paraformaldehyde dissolved in 0.1 M NaCacodylate and DRAQ5 nuclear stain was used to visualize cell nuclei (ThermoFisher Scientific, Waltham, MA). Imaging was conducted on an Olympus Fluoview FV-1000 confocal fluorescent microscope with a Super Apochromat UPLSAPO 20X objective or a Super Apochromat UPLSAPO 60×W objective. The GFP and DRAQ5 images were then merged using the open access ImageJ software and utilizing the Open Microscopy Environment Bio-Formats software plugin tool.

Statistics

The data are presented as the mean ± standard deviation (±SD). Statistical analysis was conducted using a two-tailed *t*-test and a P value ≤ 0.05 was considered significant.

Results

Fggy is induced during skeletal muscle atrophy

To identify genes that are differentially expressed in response to neurogenic atrophy, RNA was harvested from the triceps surae (TS) muscle of mice following 3 and 14 days of denervation as previously described (Furlow et al., 2013). A significant number of genes that have not previously been studied in skeletal muscle were shown to be differentially expressed in response to neurogenic skeletal muscle atrophy, including Fggy carbohydrate kinase domain containing (Fggy). At 3-days post denervation, Fggy showed a small but significant increase in expression

compared to control muscles while at 14-days post denervation, the increase in Fggy expression was greater compared to the control muscles (Fig. 8).

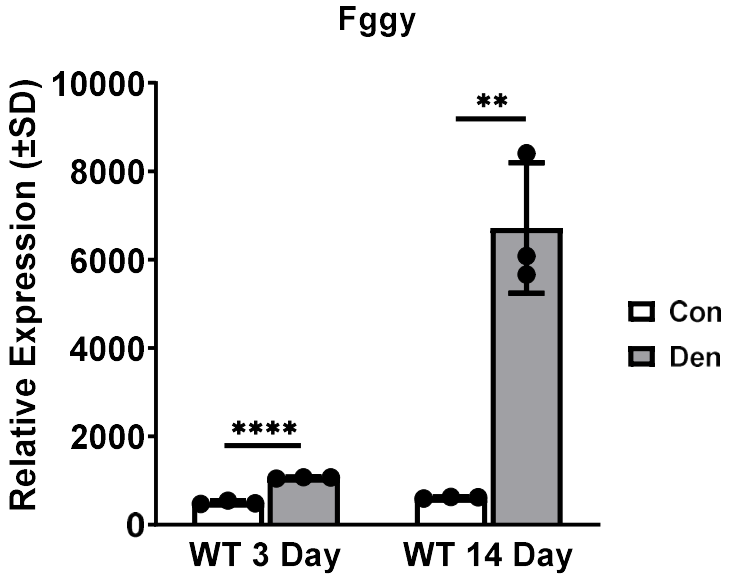

Figure 8. Fggy is induced in response to denervation-induced skeletal muscle atrophy. Whole genome expression analysis was conducted on triceps surae muscle from wild-type (WT) mice after 3 days (3D) and 14 days (14D) of denervation (DEN). Each condition represents the average expression from three animals and error bars represent ± SD. White bars represent the controls and gray bars represent DEN. Significant difference between denervated mice and control mice in the same group, $P < 0.05$. Fggy-L was recognized by a probe on exon 16 and expression showed a significant increase in atrophic conditions at 3D and 14D post denervation.

Fggy-L and Fggy-S are alternatively spliced in muscle cells

Fggy has been shown to be most abundantly expressed in liver but is also found to be expressed in skeletal muscle (Fagerberg et al., 2014), which is not unexpected considering this gene may play a role in carbohydrate metabolism. This study is the first to identify four alternative Fggy isoforms simultaneously expressed in muscle cells, two of which are completely novel (Fig. 9A-B). We have designated these four isoforms as Fggy-Long form, which consists of 552 amino acids (Fggy-L-552), an alternative Fggy-Long form consisting of 482 amino acids (Fggy-L-482), Fggy-Short form consisting of 387 amino acids (Fggy-S-387), and an alternative Fggy-Short form consisting of 344 amino acids (Fggy-S-344) (Fig. 9A-B). The two novel transcripts are shorter

than their previously identified counterparts with Fggy-L-482 lacking exons 10 and 11 and Fggy-S-344 lacking exon 7 (Fig. 9A-B). The Fggy-S-387 isoform differs from the Fggy-L-552 isoform at amino acids 360 to 387 and is lacking amino acids 388-552. Bioinformatic analysis of the Fggy gene in both humans and rodents revealed a locus that generates numerous splice variants and has 8 putative protein encoding isoforms in mice that result from alternative splicing and/or alternative transcription initiation sites. Of the 8 putative protein encoding transcripts of the murine Fggy gene, 2 have been added to the CCDS database. The first isoform we have designated as Fggy-L-552 (CCDS51233), which consists of 16 exons and 15 introns and has a predicted molecular weight of approximately 60 kDa. The second isoform we have designated as Fggy-S-387 (CCDS18365), which consists of 11 exons and 10 introns and produces a protein with a predicted molecular weight of approximately 42.5 kDa. Interestingly, both isoforms retain the conserved FGGY-N and FGGY-C domains characteristic of the FGGY carbohydrate kinase family.

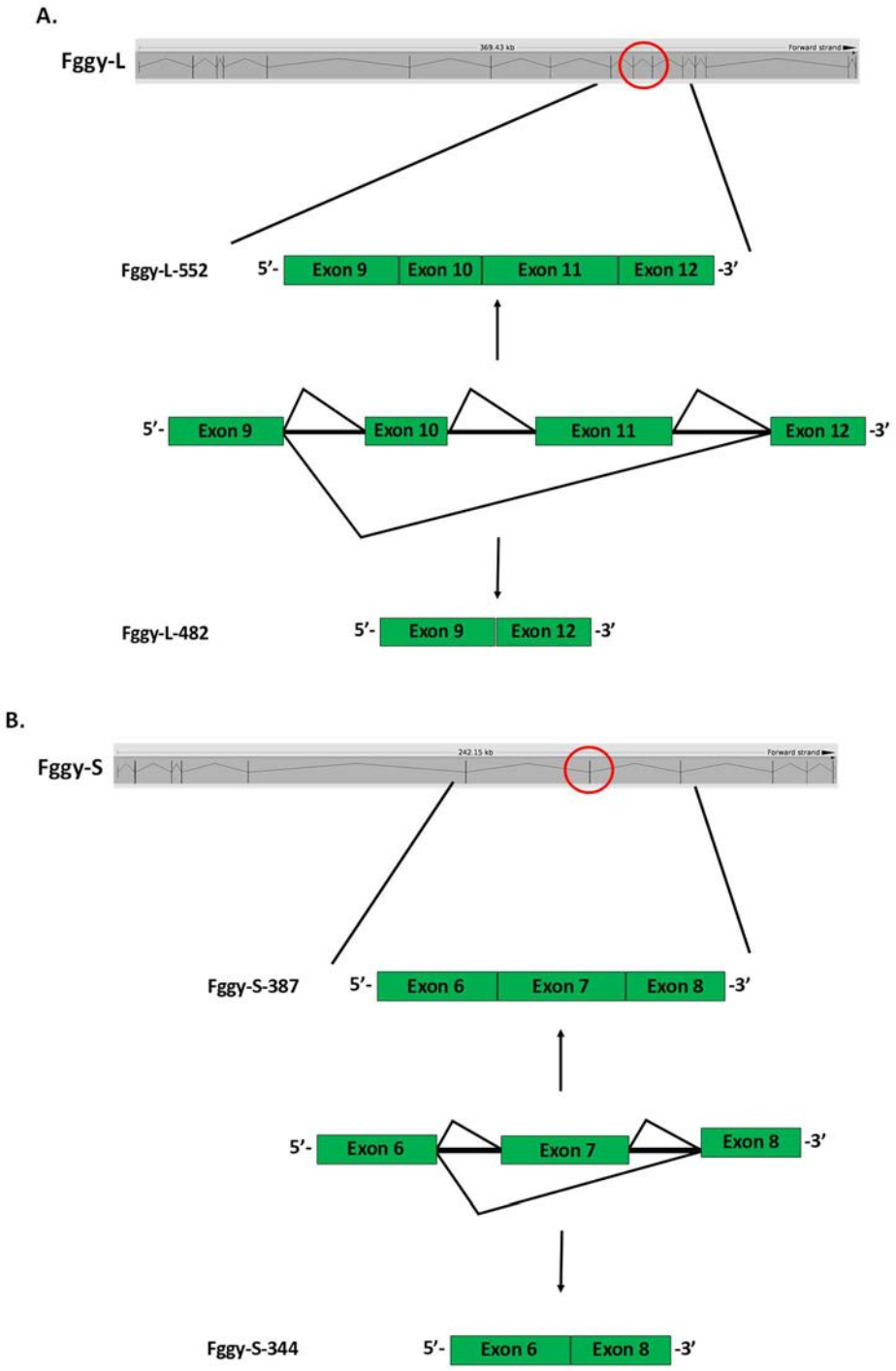

Figure 9. Schematics of alternative transcripts of Fggy-L and Fggy-S. (A) Fggy-L-552 has 16 exons and 15 introns and an alternative transcript without exons 10 and 11 (red circle) named Fggy-L-482 for the number of amino acids in the protein sequence. The schematic of the Fggy genes structure was downloaded from the Ensembl database (www.ensembl.org)**.** (B) Fggy-S-387 has 11 exons and 10 introns and an alternative transcript without exon 7 (red circle) named Fggy-S-344. The schematic of the Fggy genes structure was downloaded from the Ensembl database (www.ensembl.org).

Fggy-L is upregulated during muscle cell differentiation

To analyze the expression profile of Fggy in proliferating myoblasts and differentiated myotubes, qPCR primers were designed distinguish between the four alternative splice variants. C_2C_{12} cells were harvested at proliferation day 2 (PD2), differentiation day 2 (DD2), and differentiation day 7 (DD7). RNA was isolated and used for analysis of Fggy expression by reverse transcription quantitative polymerase chain reaction (RT-qPCR). The results show that the expression of the Fggy-L isoforms peak during early differentiation (Fig. 10A-B), while the expression of the Fggy-S isoforms remains relatively constant between proliferation and differentiation (Fig. 10C-D).

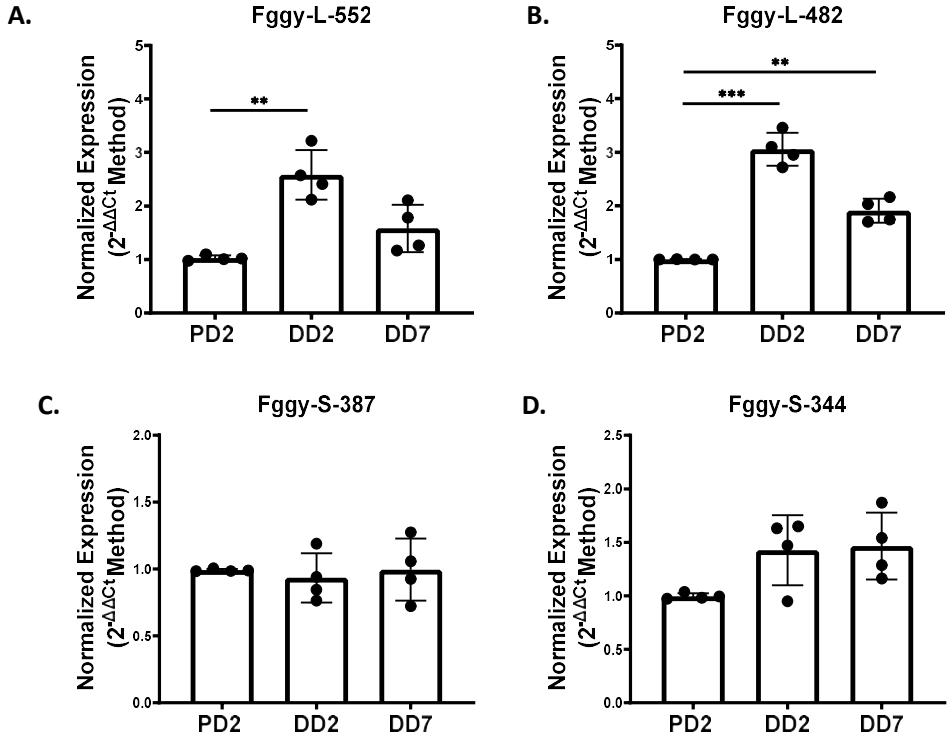

Figure 10. Expression pattern analysis of the Fggy isoforms in cultured muscle cells. RT-qPCR analysis of the (A) Fggy-L-552, (B) Fggy-L-487, (C) Fggy-S-384, and (D) Fggy-S-344 transcripts in proliferating (PD2) myoblasts and early (DD2) and late differentiated (DD7) myotubes. Significant difference between proliferating (PD2) and differentiated cells (**: $P < 0.01$, ***:$P < 0.001$).

Fggy localizes to the cytoplasm of myoblasts

To elucidate the sub-cellular location of Fggy in muscle cells, pEGFP-Fggy-L and pEGFP-Fggy-S expression plasmids were created and transfected into C_2C_{12} cells. The Fggy-L isoforms both show a diffuse and uniform cytoplasmic localization pattern (Fig. 11), while the Fggy-S isoforms show a more punctate cytoplasmic localization pattern (Fig. 12) These distinct localization patterns may be due to the Fggy-L isoforms possessing a 165 amino acid c-terminal tail region that is missing in the Fggy-S isoforms (Fig. 13).

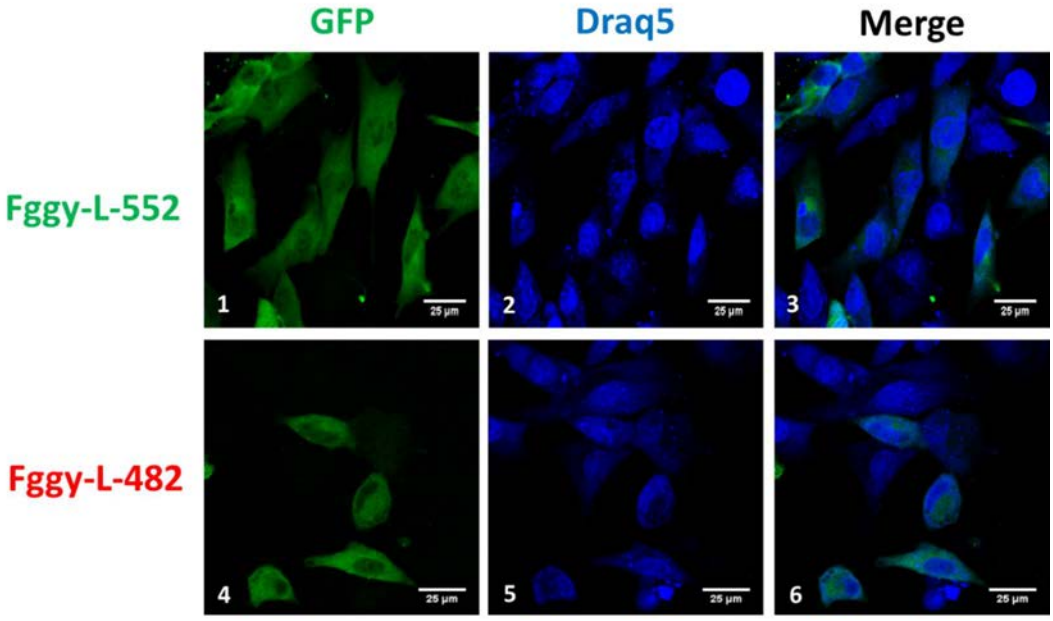

Figure 11. Fggy-L isoforms localize to the cytoplasm in C_2C_{12} cells. C_2C_{12} cells that were transfected with pEGFP-Fggy-L expression plasmids and imaged at 60X. Fggy-L-552 (Panels 1-3) and Fggy-L-482 (Panels 4-6) were found to localize to the cytoplasm of myoblasts. Nuclei were visualized using Draq5. Scale bar = 25 µm

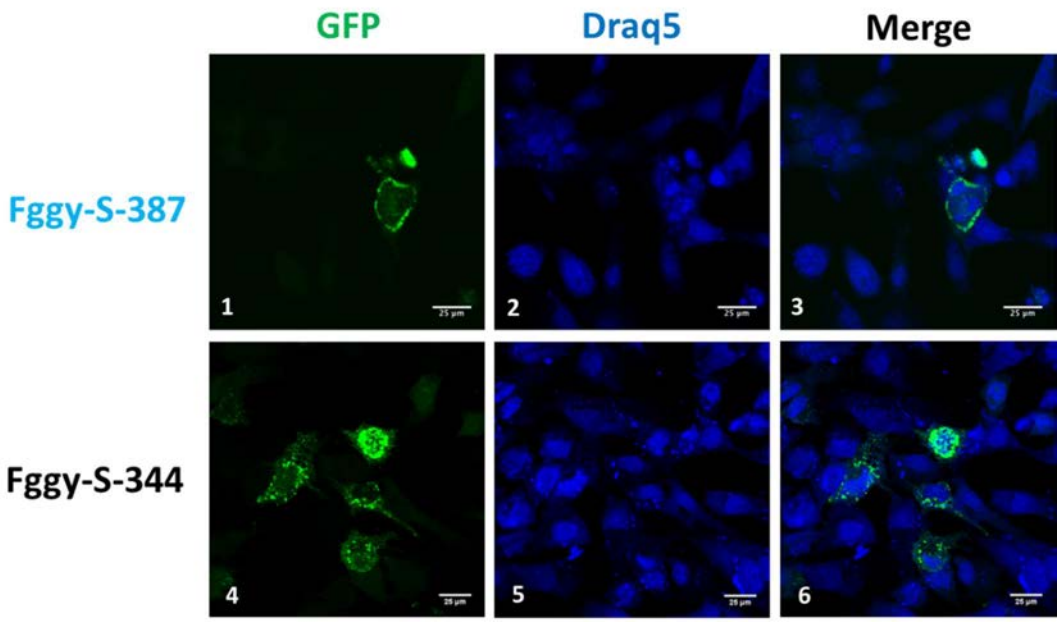

Figure 12. Fggy-S isoforms localize to the cytoplasm in a punctate pattern in C_2C_{12} cells. C_2C_{12} cells that were transfected with pEGFP-Fggy-S expression plasmids and imaged at 60X. Fggy-S-387 (Panels 1-3) and Fggy-S-344 (Panels 4-6) were found to localize in a punctate pattern to the cytoplasm of myoblasts. Nuclei were visualized using Draq5. Scale bar = 25 μm

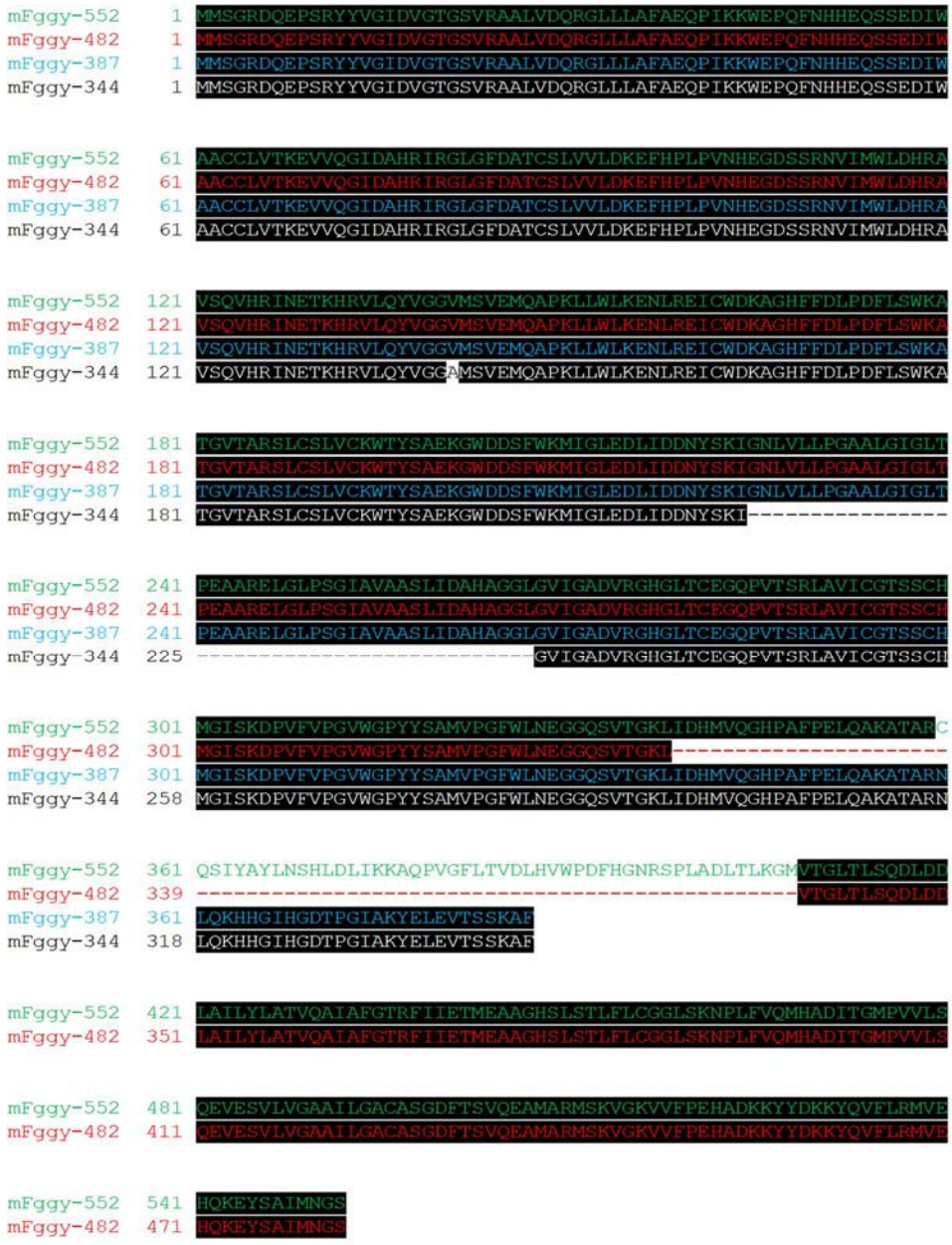

Figure 13. Alignment of the Fggy protein sequences. The amino acid sequences of the four murine Fggy isoforms aligned using the ClustalW2 algorithm and shaded using Boxshade.

Ectopic Fggy expression attenuates muscle cell differentiation

To determine the effect of Fggy overexpression on muscle cell differentiation, the pcDNA3-Fggy-L-552 and pcDNA3-Fggy-S-387 expression plasmids were used to transfect C_2C_{12} cells. The cells

were then harvested over a differentiation time course, lysed, and protein homogenates were used for Western blot analysis of known markers of muscle cell differentiation. Myosin heavy chain (MyHC) and myogenin both showed significantly blunted expression in response to ectopic expression of Fggy-L-552 and Fggy-S-387 at all differentiation timepoints (Fig. 14A and 15A). To confirm Fggy-mediated inhibition of muscle cell differentiation, biological quadruplicates of Fggy-L-552 or Fggy-S-387 overexpressing cells were harvested at differentiation day 2 and analyzed by Western blot (Fig. 14B and 15B). Quantification of the Western blots for MyHC and myogenin protein levels confirmed a statistically significant reduction in both (Fig. 14C and 15C). GAPDH expression was analyzed to verify equal protein loading.

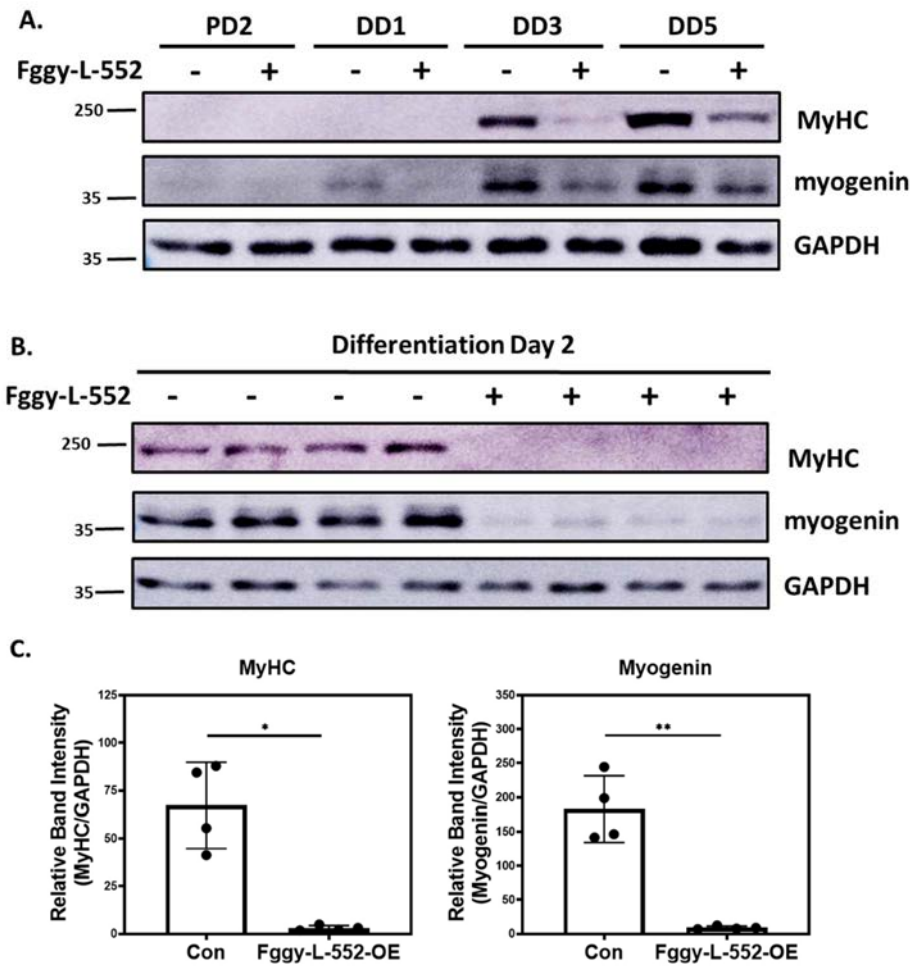

Figure 14. Ectopic expression of Fggy-L attenuates muscle cell differentiation. C_2C_{12} cells were transfected with the pcDNA-Fggy-L-552 expression plasmid. Cells were maintained in 10% serum media for the proliferation timepoints and switched to 2% serum media to induce differentiation. Cells were harvested at proliferation day 2 (PD2) and differentiation days 1, 3, and 5 (DD1, DD3, DD5). (A) Western blot analysis of the differentiation markers Myosin Heavy Chain (MyHC) and myogenin showed significantly lower levels of expression at DD3 and DD5 in response to Fggy-L-552 overexpression. (B) C_2C_{12} cells were transfected with the pcDNA-Fggy-L-552 expression plasmid in biological quadruplicates, maintained in proliferation media, and then switched to differentiation media (2% serum) for 2 days. Western blot analysis of MyHC and myogenin using protein homogenates from C_2C_{12} cells differentiated for 2 days. (C) Quantification of the Western blot band intensities from part B. Relative intensity of each band was corrected to the GAPDH band intensity for each corresponding biological replicate. Significant differences between control cells compared to cells ectopically expressing Fggy-L-552, (*: $P < 0.05$, **: $P < 0.01$).

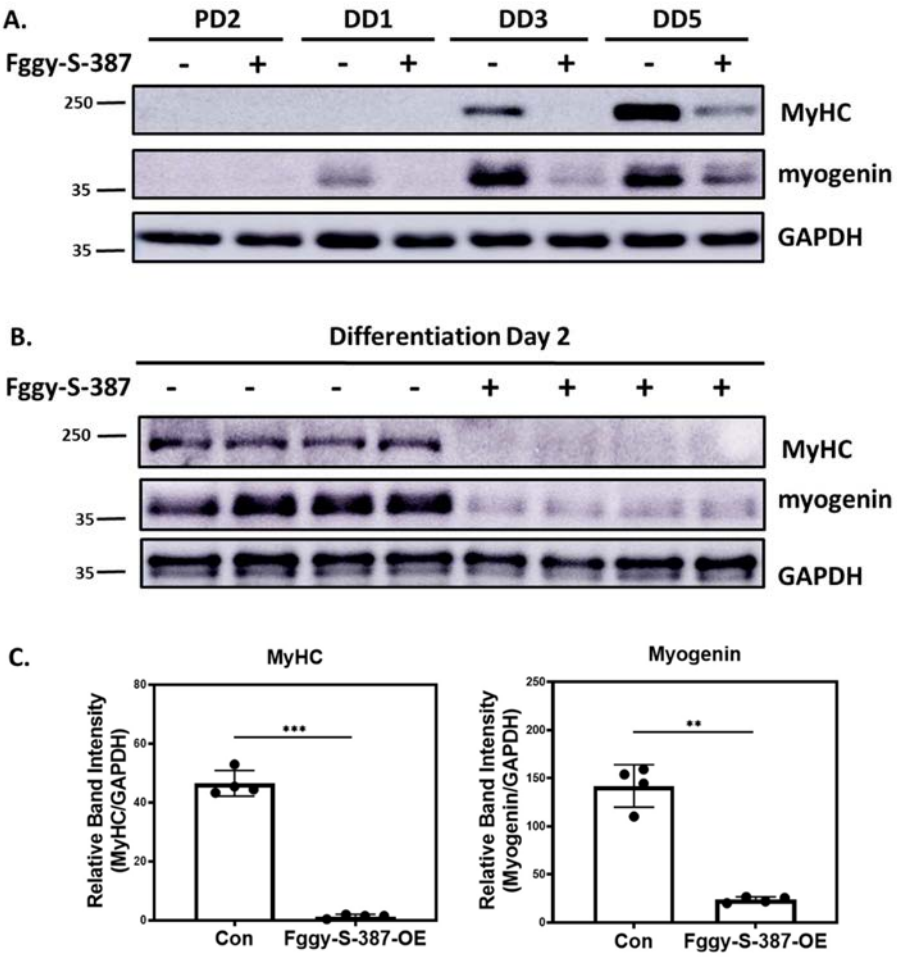

Figure 15. Ectopic Fggy-S expression attenuates muscle cell differentiation. C_2C_{12} cells were transfected with the pcDNA-Fggy-S-387 expression plasmid. Cells were maintained in 10% serum media for the proliferation timepoints and switched to 2% serum media to induce differentiation. Cells were harvested at proliferation day 2 (PD2) and differentiation days 1, 3, and 5 (DD1, DD3, DD5). (A) Western blot analysis of the differentiation markers Myosin Heavy Chain (MyHC) and myogenin showed significantly lower levels of expression at DD3 and DD5 in response to Fggy-S-387 overexpression. (B) C_2C_{12} cells were transfected with the pcDNA-Fggy-S-387 expression plasmid in biological quadruplicates, maintained in proliferation media, and then switched to differentiation media (2% serum) for 2 days. Western blot analysis of MyHC and myogenin using protein homogenates from C_2C_{12} cells differentiated for 2 days. (C) Quantification of the Western blot band intensities from part B. Relative intensity of each band was corrected to the GAPDH band intensity for each corresponding biological replicate. Significant differences between control cells compared to cells ectopically expressing Fggy-L-552, (**: $P < 0.01$, ***: $P < 0.001$).

Fggy overexpression inhibits MAPK signaling

To evaluate the impact of Fggy overexpression on pathways critical for muscle cell differentiation, Fggy-L-552, Fggy-L-482, Fggy-S-387, and Fggy-S-344 were overexpressed individually in C_2C_{12} cells along with an activator protein-1 (AP-1) reporter gene plasmid. As one of the terminal targets of the MAPK signaling pathway, AP-1 activity can be used to measure the activity of the MAPK signaling pathway. Culture media was harvested, and SEAP activity was measured, revealing that all four Fggy isoforms inhibited MAPK signaling (Fig. 16). Phosphorylation levels of ERK1/2 were then analyzed via western blot. Phosphorylated ERK1/2 (p-ERK1/2) levels were found to be lower in cells ectopically expressing Fggy-L-552 (Fig. 17A) or Fggy-S-387 (Fig. 18A). To confirm inhibition of ERK1/2 phosphorylation levels, biological quadruplicates of Fggy-L-552 or Fggy-S-387 overexpressing cells were harvested at differentiation day 2 and analyzed by Western blot (Fig. 17B and 18B). Quantification of the Western blots for ERK1/2 protein and p-ERK1/2 levels confirmed a statistically significant reduction in phosphorylated ERK1/2 (Fig. 17C and 18C).

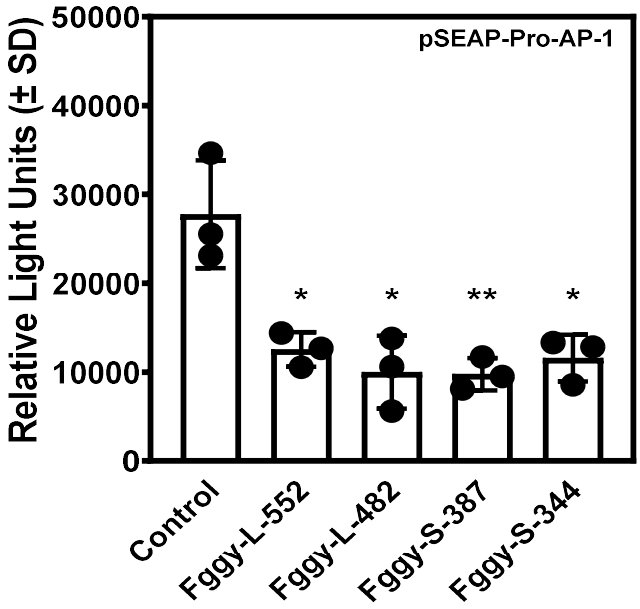

Figure 16. Ectopic expression of Fggy inhibits MAPK signaling. C_2C_{12} cells were transfected with pcDNA3-Fggy-L-552, pcDNA3-Fggy-L-482, pcDNA3-Fggy-S-387, or pcDNA3-Fggy-S-344 expression plasmids along with a MAP kinase signaling pathway reporter gene. SEAP activity

was measured by harvesting culture media 72 hours post-media change. Cells ectopically expressing Fggy showed significantly less SEAP activity. (*:P < 0.05, **:P < 0.01)

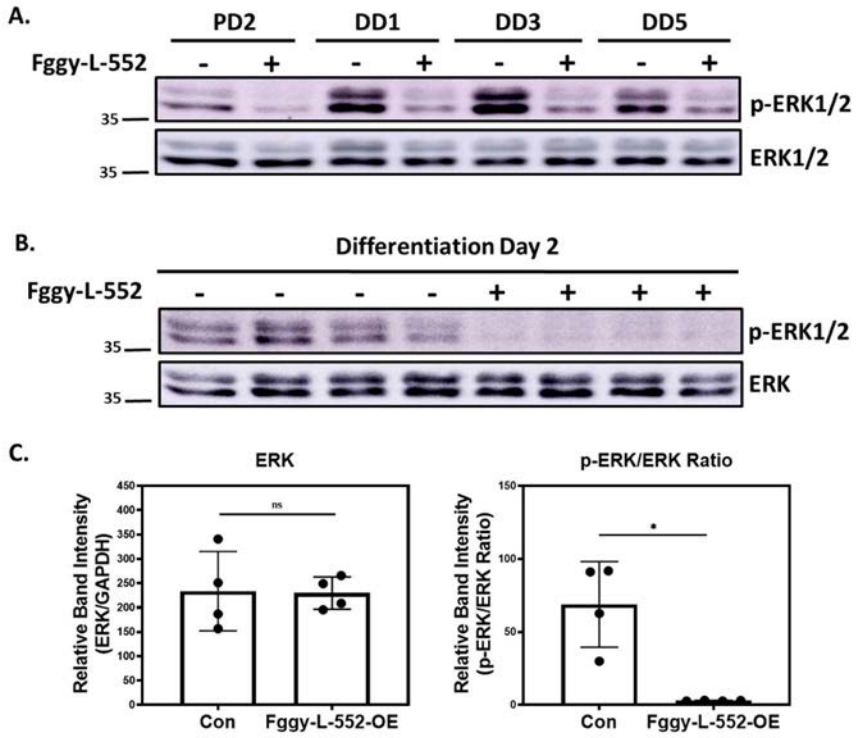

Figure 17. Ectopic expression of Fggy-L inhibits the ERK1/2 branch of the MAPK signaling cascade. C_2C_{12} cells were transfected with the pcDNA-Fggy-L-552 expression plasmid. Cells were maintained in 10% serum media for the proliferation timepoints and switched to 2% serum media to induce differentiation. Cells were harvested at proliferation day 2 (PD2) and differentiation days 1, 3, and 5 (DD1, DD3, DD5). (A) Western blot analysis of ERK1/2 and phospho-ERK1/2 showed significantly lower levels at all time points in response to Fggy-L-552 overexpression. (B) C_2C_{12} cells were transfected with the pcDNA-Fggy-L-552 expression plasmid in biological quadruplicates, maintained in proliferation media, and then switched to differentiation media (2% serum) for 2 days. Western blot analysis of ERK1/2 and phosphor-ERK1/2 using protein homogenates from C_2C_{12} cells differentiated for 2 days. (C) Quantification of the Western blot band intensities from part B. Relative intensity of each band was corrected to the GAPDH band intensity for each corresponding biological replicate. Significant differences between control cells compared to cells ectopically expressing Fggy-L-552, (*: $P < 0.05$, ns = no significance).

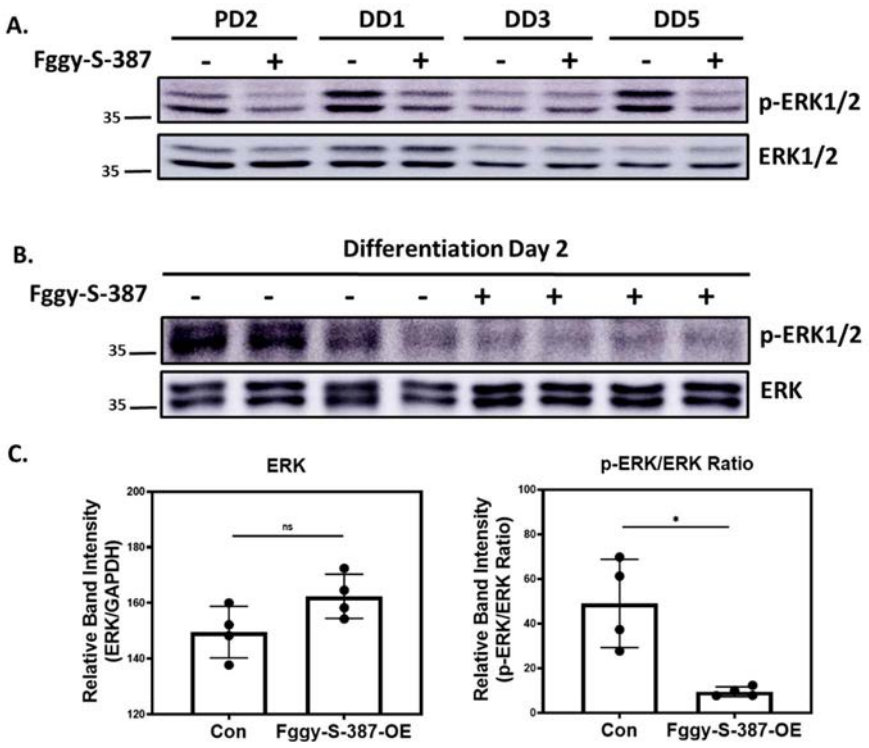

Figure 18. Ectopic expression of Fggy-S inhibits the ERK1/2 branch of the MAPK signaling cascade. C_2C_{12} cells were transfected with the pcDNA-Fggy-S-387 expression plasmid. Cells were maintained in 10% serum media for the proliferation timepoints and switched to 2% serum media to induce differentiation. Cells were harvested at proliferation day 2 (PD2) and differentiation days 1, 3, and 5 (DD1, DD3, DD5). (A) Western blot analysis of ERK1/2 and phospho-ERK1/2 showed significantly lower levels at all time points except DD3 in response to Fggy-S-387 overexpression. (B) C_2C_{12} cells were transfected with the pcDNA-Fggy-S-387 expression plasmid in biological quadruplicates, maintained in proliferation media, and then switched to differentiation media (2% serum) for 2 days. Western blot analysis of ERK1/2 and phosphor-ERK1/2 using protein homogenates from C_2C_{12} cells differentiated for 2 days. (C) Quantification of the Western blot band intensities from part B. Relative intensity of each band was corrected to the GAPDH band intensity for each corresponding biological replicate. Significant differences between control cells compared to cells ectopically expressing Fggy-L-552, (*: $P < 0.05$, ns = no significance).

Overexpression of Fggy destabilizes AKT

In addition to the MAPK signaling pathway, AKT has been found to modulate muscle cellular differentiation (Coleman et al., 1995). In response to Fggy-L-552 and Fggy-S-387 overexpression, AKT protein and phosphorylation levels were found to be significantly lower over a differentiation time course (Fig. 19A and 20A). To confirm AKT destabilization and inhibition of AKT

phosphorylation levels, biological quadruplicates of Fggy-L-552 or Fggy-S-387 overexpressing cells were harvested at differentiation day 2 and analyzed by Western blot (Fig. 19B and 20B). Quantification of the Western blots for AKT protein and p-AKT levels confirmed a statistically significant reduction in both AKT protein levels and phosphorylated AKT (Fig. 19C and 20C).

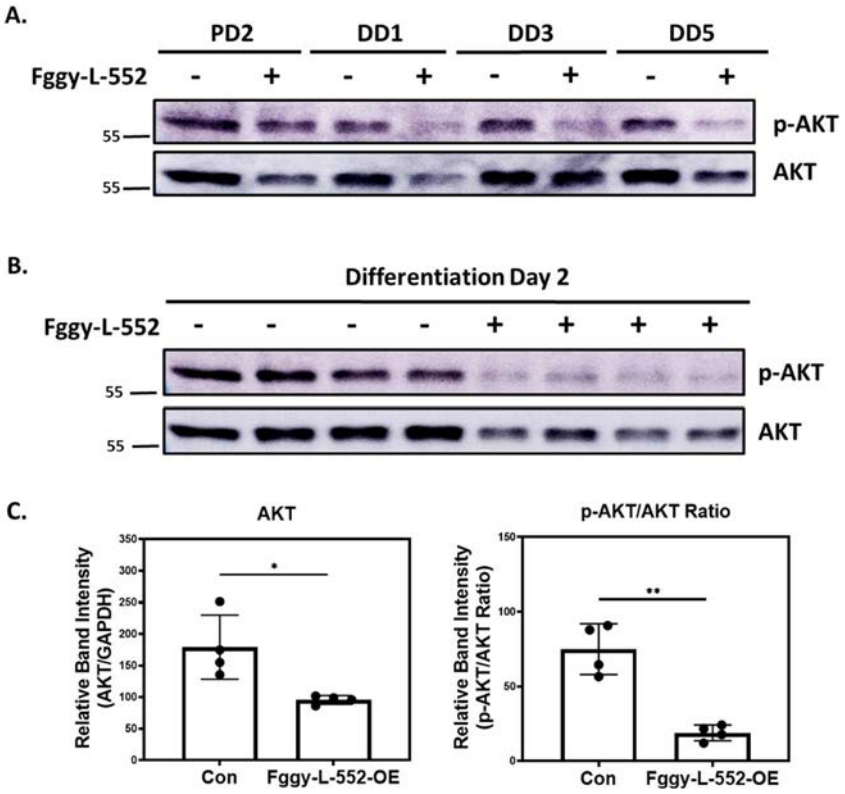

Figure 19. Ectopic expression of Fggy-L destabilizes AKT in muscle cells. C_2C_{12} cells were transfected with the pcDNA-Fggy-L-552 expression plasmid and harvested at proliferation day 2 (PD2) and differentiation days 1, 3, and 5 (DD1, DD3, DD5). (A) Western blot analysis showed reduced levels of phosphorylated AKT with Fggy over expression at all timepoints. (B) C_2C_{12} cells were transfected with the pcDNA-Fggy-L-552 expression plasmid in biological quadruplicates, maintained in proliferation media, and then switched to differentiation media (2% serum) for 2 days. Western blot analysis of p-AKT and AKT using protein homogenates from C_2C_{12} cells differentiated for 2 days. (C) Quantification of the Western blot band intensities from part B. Relative intensity of each band was corrected to the GAPDH band intensity for each corresponding biological replicate. Significant differences between control cells compared to cells ectopically expressing Fggy-L-552, (*: $P < 0.05$,**: $P < 0.01$).

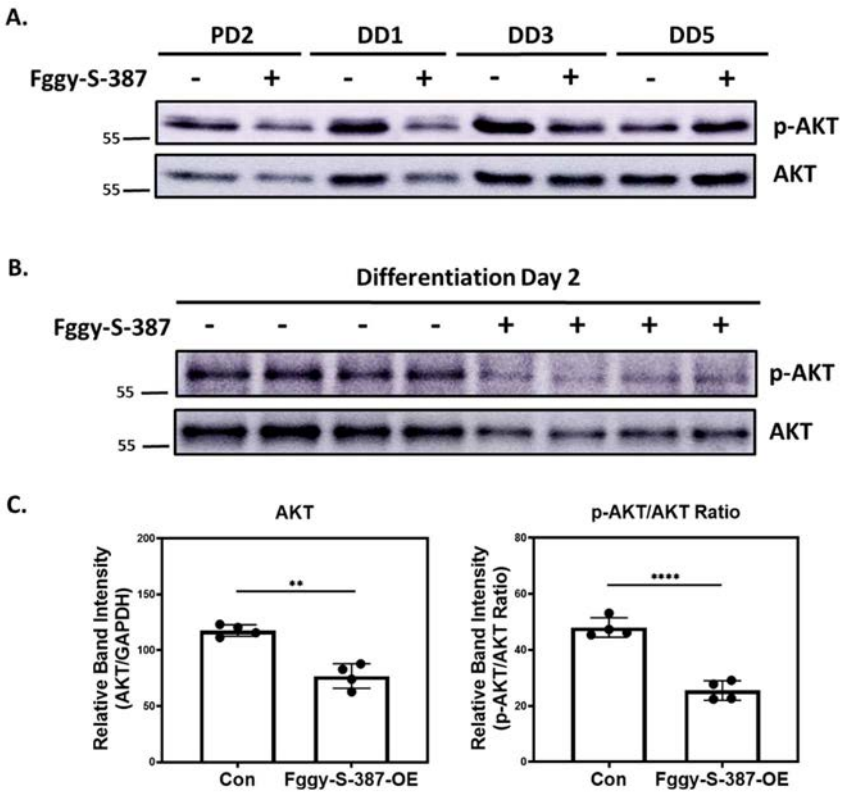

Figure 20. Ectopic expression of Fggy-S destabilizes AKT in muscle cells. C_2C_{12} cells were transfected with the pcDNA3-Fggy-S-387 expression plasmid and harvested at proliferation day 2 (PD2) and differentiation days 1, 3, and 5 (DD1, DD3, DD5). (A) Western blot analysis showed lower levels of phosphorylated AKT with Fggy overexpression at all timepoints except DD5. (B) C_2C_{12} cells were transfected with the pcDNA-Fggy-S-387 expression plasmid in biological quadruplicates, maintained in proliferation media, and then switched to differentiation media (2% serum) for 2 days. Western blot analysis of p-AKT and AKT using protein homogenates from C_2C_{12} cells differentiated for 2 days. (C) Quantification of the Western blot band intensities from part B. Relative intensity of each band was corrected to the GAPDH band intensity for each corresponding biological replicate. Significant differences between control cells compared to cells ectopically expressing Fggy-S-387, (**: $P < 0.01$, ****: $P < 0.0001$).

Discussion

Fggy may regulate muscle cell differentiation through modulation of the MAPK pathway

The levels of Fggy-L transcript were highest during differentiation, leading us to investigate the effect of ectopic expression of Fggy on the induction of MyHC and myogenin during muscle cell differentiation. In this study, we found that Fggy overexpression resulted in the inhibition of both MyHC and myogenin expression, suggesting attenuation of muscle cell differentiation. Although this data provides evidence that Fggy may play a role in proper muscle cell differentiation, it also suggests a more complex interaction with myogenin, since myogenin expression also increases in response to skeletal muscle atrophy induced by denervation (Moresi et al., 2010, Furlow et al., 2013). The mechanism by which Fggy inhibits muscle differentiation remains to be fully elucidated; however, we did find that overexpression of any of the Fggy isoforms was sufficient to inhibit the MAPK signaling pathway. It has previously been shown that MAP kinase signaling is necessary for the proper differentiation of myotubes (Cooper et al., 1982) and may occur through any of four distinct branches, including the extracellular signal-related kinase 1/2 (ERK1/2), p38, c-Jun N-terminal kinase (JNK), or ERK5 (Cargnello and Roux, 2011). Therefore, we wanted to determine which of these branches might be regulated by Fggy and, based on previous studies from our lab, we hypothesized that Fggy may target the ERK1/2 branch in muscle cells (Haddock et all, 2019, Hayes et al., 2019, Cooper et al., 2020, Labuzan et al., 2020). Western blot analysis showed that Fggy overexpression in C_2C_{12} cells decreased phosphorylation of ERK1/2 and inhibited an AP-1 reporter gene. The ERK1/2 branch varies in activity during the progression from myoblast to myotube and finally to myotube fusion. ERK1/2 phosphorylation is highest during proliferation and late differentiation and plays a role in both the initiation of myogenesis and myotube fusion (Bennett and Tonks, 1997). The results from this current study, showing that

overexpression of Fggy may attenuate the MAPK pathway, suggest a possible mechanism by which Fggy functions in regulating muscle cell differentiation.

Fggy may contribute to protein degradation through AKT inhibition

The AKT pathway is also involved in muscle cell differentiation and Fggy overexpression was shown to decrease protein and phosphorylation levels of AKT. Interestingly, a previous study found that elevated levels of Fggy expression in adipose tissue were positively correlated with obesity in male mice exposed to low doses of BPA (Taylor et al., 2018). Due to their coordinated role in energy metabolism, the relationship between adipose tissue and skeletal muscle is well established if not fully understood. Indeed, a recent study showed that transplantation of adipose tissue from mice that regularly trained on a running wheel into sedentary mice resulted in improved insulin-stimulated glucose uptake in the skeletal muscle of the sedentary mice (Stanford et al., 2015). Insulin induced AKT signaling modulates adipose tissue metabolism by increasing cellular glucose uptake, protein synthesis, and synthesis of new fatty acids (Zhang and Liu, 2014). The involvement of AKT in lipid and glucose metabolism provides a possible method by which Fggy may participate in the regulation of fat deposition. Taylor et al. found evidence of a positive relationship between Fggy expression and levels of adipose tissue, while our data showed that increased Fggy expression decreases AKT expression. While these findings, might seem contradictory as the activation of AKT leads to the synthesis of new fatty acids, Fggy may have a muscle specific function that differs from its role in adipose tissue. In 2019 it was found that obese adipose tissue accelerated denervation-induced muscle atrophy through FoxO activation and an increased expression of FoxO target genes associated with atrophy (Zhu et al, 2019). This data also supports the hypothesis that induction of Fggy during muscle atrophy may lead to the negative regulation of AKT signaling and block AKT-mediated inhibition of the transcriptional activation

of atrophy-promoting genes, including MuRF1 and MAFbx. The activation of these genes may then lead to protein degradation, muscle wasting, and weakness, further suggesting that the increase in Fggy expression in response to denervation may contribute to muscle wasting

Future Directions

Characterize the regulation of Fggy splice variant expression in muscle cells

The identification and characterization of Fggy in skeletal muscle expands our understanding of the molecular mechanisms of skeletal muscle atrophy. In this study, we found that the Fggy gene produces two novel transcripts in skeletal muscle in addition to two transcripts that have previously been validated. The expression of these novel transcripts in skeletal muscle suggests that Fggy may have a muscle specific function. The levels of the two Fggy-L transcripts were found to be increased during differentiation, while the two Fggy-S transcripts did not change significantly between proliferation and differentiation. Proper muscle cell differentiation is regulated by the expression of myogenic regulatory factors (MRF's), with MyoD and Myogenin found to be most active during early myoblast differentiation (Bentzinger et al., 2012). MRF's function by binding to a DNA sequence, called an E-box, with their conserved helix-loop-helix domain. These binding sequences are often found in the promoter regions of muscle-specific genes (Berkes and Tapscott, 2005). Both MyoD and myogenin have also been shown to increase in expression during neurogenic skeletal muscle atrophy (Merlie et al., 1994). The upregulated expression of the Fggy gene in skeletal muscle during early differentiation and during neurogenic skeletal muscle atrophy suggests that the increase in MyoD or myogenin may participate in the upregulation of Fggy expression during muscle atrophy. Moreover, future investigation of the differential splicing of Fggy during muscle cell development could determine if expression of specific MRF's promotes

expression of one isoform over another during muscle cell growth and differentiation. A better understanding of the regulation of Fggy in muscle will help to improve our knowledge of the functions that the different isoforms of Fggy play in muscle development and atrophy.

Fggy may function within the pentose phosphate pathway

The pentose phosphate pathway, also known as the phosphogluconcate pathway, generates NADPH and molecules necessary for nucleotide synthesis (Alfarouk et al., 2020). While the liver is found to have one of the highest levels of PPP activity (Heinrich et al., 1976), denervation-induced skeletal muscle atrophy causes an increase in levels of PPP activity specifically in muscle cells (Wagner et al., 1977). This study linked the regeneration of skeletal muscle with enzymatic activity of the PPP using a myotoxic local anesthetic called Marcaine that promotes rapid regeneration of muscle tissue (Benoit and Belt, 1970). In humans, Fggy has been found to be expressed highest in the liver (Fagerberg et al., 2014). This correlates with a previous study that found Fggy may function as a D-ribulokinase in HEK293 cells, suggesting that the role of this enzyme may be to phosphorylate free D-ribulose to prevent toxic accumulation (Singh et al., 2017), as free D-ribulose is not found to be abundant in mammalian cells but is found in human and rat urine (Futterman and Roe, 1955). It was also found that YDR109C, the yeast homolog of Fggy, showed a substrate preference to D-ribulose (Singh et al., 2017). Interestingly, the Molecular INTeraction (MINT) data base provides evidence of an interaction between Fggy and 6-phosphogluconolactonase (Pgls) which, along with D-ribulose, has been identified as a component of the pentose phosphate pathway (PPP). In the context of skeletal muscle atrophy, the previous data suggests Fggy may play a role in the pentose phosphate pathway as the body attempts to regenerate atrophied muscle tissue. As the PPP activity increases in muscle, the need to phosphorylate D-ribulose for use in this pathway also increases, which could account for the

increase in Fggy expression. This potential role for Fggy in skeletal muscle could be investigated through the mutagenesis of regions predicted to interact with D-ribulose based on structural homology models of the yeast Ydr109c and human FGGY proteins. It would be possible to compare the amount of free ribulose in C_2C_{12} cells in response to ectopic expression of wild-type and mutant Fggy, as well as, in response to Fggy expression knockdown. These studies could determine if C_2C_{12} cells contain enough free ribulose to be detected and if there are changes in those levels in response to an increase or decrease in Fggy expression, as well as, if the kinase activity of Fggy is necessary for ribulose phosphorylation. As it has not yet been determined which mutation will result in a kinase dead Fggy protein, multiple mutations would have to be tested and the amount of free ribulose measured in order to show the loss of activity. This could be done by site-directed mutagenesis of conserved amino acids identified in 12 organisms across different kingdoms of life (Fig. 21) (Singh et al, 2017) or through truncating the Fggy gene until a change in activity is achieved, such as deletion of either the Fggy-N or Fggy-C functional domains which are located at the N and C termini, respectively (Fig. 22).

Figure 21. Alignment of D-ribulokinase protein sequences across different kingdoms of life. Conserved amino acids are highlighted in increasingly darker shades of blue relative to a higher degree of conservation. The top 20 specificity determining positions (SDPs) are highlighted in red. The amino acids that are predicted to interact with the pentose substrate are highlighted in yellow. This is based on structural homology models of the yeast Ydr109c and human FGGY proteins (Singh et al., 2017).

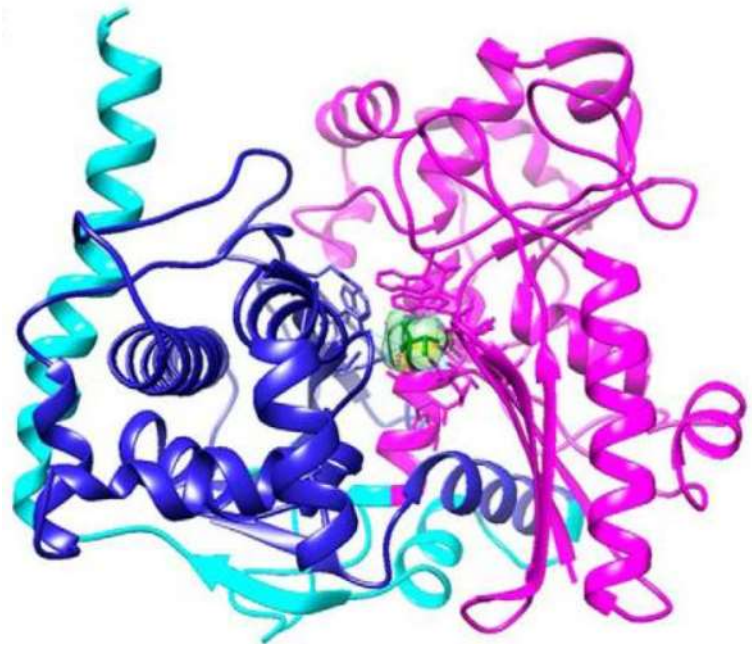

Figure 22. Model of the human Fggy protein. Shown in complex with the ligand d-xylulose (light green color). The Fggy-C domain is highlighted in dark blue and Fggy-N domain is highlighted in pink (Singh et al., 2017).

Fggy may interact with deubiquitinases

Although Fggy was found to be correlated with instances of sporadic amyotrophic lateral sclerosis (S-ALS) (Dunckley et al., 2007), multiple other studies found no evidence to support this finding (Daoud et al., 2012 and Cai et al., 2014). Interestingly, Fggy has been predicted to interact with two deubiquitinases, Myb-like, SWIRM, and MPN domains-containing protein 1 (MYSMP1) and Ubiquitin-specific protease 24 (USP24) (Jensen et al., 2008). MYSMP1 has been shown to act as a transcriptional activator by releasing the inhibition caused by ubiquitination of histone 2A (H2A) (Zhu et al., 2007). In addition, USP24 has been implicated in apoptosis and iron metabolism responsible for avoiding cell death (Sun et al., 2018). USP24 has also been found to deubiquitinate p53, which is necessary for the stabilization of p53 expression (Zhang et al., 2015). This is interesting as USP24 is found to decrease 7 days after denervation in gastrocnemius muscle tissue (Lang et al., 2017), while p53 is found to increase in expression 7 days after denervation in tibialis

anterior muscle (Stouth et al., 2020). Skeletal muscle atrophy has been shown to cause an increase in the expression of various deubiquitinases, which is thought to compensate for the increased demand for ubiquitin that is needed to target proteins for degradation by the proteasome (Wing, 2013). Moreover, the removal of ubiquitin tags from some substrates may also disrupt normal protein-protein interactions and complex formation and allow for ubiquitination of complexed proteins by E3 ligases eventually leading to their destruction by the proteasome. Further investigation into possible interactions between Fggy and USP24 and MYSMP1 through co-immunoprecipitation assays will provide a more complete understanding of the functional role of Fggy in the molecular mechanisms of skeletal muscle atrophy. The finding that Fggy shows increased expression under neurogenic atrophy inducing conditions is just one step to understanding how skeletal muscle adapts to physiological changes.

References

Adi S, Bin-Abbas B, Wu NY, Rosenthal SM. Early Stimulation and Late Inhibition of Extracellular Signal-Regulated Kinase 1/2 Phosphorylation by IGF-I: A Potential Mechanism Mediating the Switch in IGF-I Action on Skeletal Muscle Cell Differentiation. *Endocrinology*. 2002; 143(2): 511–516.

Alessi DR, Andjelkovic M, Caudwell B, Cron P, Morrice N, Cohen P, Hemmings BA. Mechanism of activation of protein kinase B by insulin and IGF-1. EMBO J. 1996 Dec 2;15(23):6541-51. PMID: 8978681; PMCID: PMC452479.

Alfarouk KO, Ahmed SBM, Elliott RL, Benoit A, Alqahtani SS, Ibrahim ME, Bashir AHH, Alhoufie STS, Elhassan GO, Wales CC, Schwartz LH, Ali HS, Ahmed A, Forde PF, Devesa J, Cardone RA, Fais S, Harguindey S, Reshkin SJ. The Pentose Phosphate Pathway Dynamics in Cancer and Its Dependency on Intracellular pH. *Metabolites*. 2020; 10(7):285.

Baracos VE, DeVivo C, Hoyle DH, Goldberg AL. Activation of the ATP-ubiquitin-proteasome pathway in skeletal muscle of cachectic rats bearing a hepatoma. Amer J Physiol Endo Metab. 1995;268:E996–E1006.

Bennett, A.M., Tonks, N.K. 1997 Regulation of Distinct Stages of Skeletal Muscle Differentiation by Mitogen-Activated Protein Kinases. *Science*. 278(5341): 1288-1291

Benoit PW, Belt WD. Destruction and regeneration of skeletal muscle after treatment with a local anaesthetic, bupivacaine (Marcaine). J Anat. 1970 Nov;107(Pt 3):547-56. PMID: 5492943; PMCID: PMC1233878.

Bentzinger C, Wang Y, Rudnicki M. Building Muscle: Molecular Regulation of Myogenesis. Cold Spring Harb. Perspect. Biol. 2012.4:a008342

Berkes CA, Tapscott SJ. MyoD and the transcriptional control of myogenesis. Semin Cell Dev Biol. 2005 Aug-Oct;16(4-5):585-95. doi: 10.1016/j.semcdb.2005.07.006. PMID: 16099183.

Bodine SC, Latres E, Baumhueter S, Lai VK, Nunez L, Clarke BA, Poueymirou WT, Panaro FJ, Na E, Dharmarajan K, Pan ZQ, Valenzuela DM, DeChiara TM, Stitt TN, Yancopoulos GD, Glass DJ. Identification of ubiquitin ligases required for skeletal muscle atrophy. Science. 2001 Nov 23;294(5547):1704-8. doi: 10.1126/science.1065874. Epub 2001 Oct 25. PMID: 11679633.

Bodine SC, Baehr LM. Skeletal muscle atrophy and the E3 ubiquitin ligases MuRF1 and MAFbx/atrogin-1. Am J Physiol Endocrinol Metab. 2014 Sep 15;307(6):E469-84. doi: 10.1152/ajpendo.00204.2014. Epub 2014 Aug 5. PMID: 25096180; PMCID: PMC4166716.

Borlepawar, A., Frey, N., and Rangrez, A.Y. 2018. "A systematic view on E3 ligase Ring TRIMmers with a focus on cardiac function and disease." Trends In Cardiovascular Medicine

Cai B, Tang L, Zhang N, and Fan D. Single-nucleotide polymorphism rs6690993 in FGGY is not associated with amyotrophic lateral sclerosis in a large Chinese cohort. *Neurobiol. Aging* 2014; 151 (35)

Cargnello M, Roux PP. Activation and function of the MAPKs and their substrates, the MAPK-activated protein kinases [published correction appears in Microbiol Mol Biol Rev. 2012 Jun;76(2):496]. Microbiol Mol Biol Rev. 2011;75(1):50–83. doi:10.1128/MMBR.00031-10.

Caunt CJ, Keyse SM. Dual-specificity MAP kinase phosphatases (MKPs): shaping the outcome of MAP kinase signalling. FEBS J. 2013 Jan;280(2):489-504. doi: 10.1111/j.1742-4658.2012.08716.x. Epub 2012 Aug 28. PMID: 22812510; PMCID: PMC3594966.

Coleman ME, DeMayo F, Yin KC, Lee HM, Geske R, Montgomery C, Schwartz RJ. Myogenic vector expression of insulin-like growth factor I stimulates muscle cell differentiation and myofiber hypertrophy in transgenic mice. Journal of Biological Chemistry. 1995;270:12109–12116.

Cooper J, Bowen-Pope D, Raines E, Ross R, Hunter T. Similar effects of Platelet-Derived Growth Factor Epidermal Greowth Facter on the Phosphorylation of Tyrosine in Cellular Proteins. *Cell.* 1982;31(1):263-273. doi: 10.1016/0092-8674(82)90426-3

Cooper LM, Hanson A, Kavanagh JA, Waddell DS. Fam83d modulates MAP kinase and AKT signaling and is induced during neurogenic skeletal muscle atrophy. Cell Signal. 2020 Jun;70:109576. doi: 10.1016/j.cellsig.2020.109576. Epub 2020 Feb 21. PMID: 32092437.

Cooper LM, West RC, Hayes CS, Waddell DS. Dual-specificity phosphatase 29 is induced during neurogenic skeletal muscle atrophy and attenuates glucocorticoid receptor activity in muscle cell culture. Am J Physiol Cell Physiol. 2020 Aug 1;319(2):C441-C454. doi: 10.1152/ajpcell.00200.2020. Epub 2020 Jul 8. PMID: 32639872.

Daoud H, Valdmanis PN, Dion PA, Rouleau GA. Analysis of DPP6 and FGGY as candidate genes for amyotrophic lateral sclerosis. *Amyotroph. Lateral Scler*. 2010; 11:389–391.

Dodd, R. 2011. Ubiquitylation [open access image]. Attribution: By Rogerdodd at the English language Wikipedia, CC BY-SA 3.0, https://commons.wikimedia.org/w/index.php?curid=7677277

Dunckley T, Huentelman MJ, Craig DW, Pearson JV, Szelinger S, Joshipura K, Halperin RF, Stamper C, Jensen KR, Letizia D, Hesterlee SE, Pestronk A, Levine T, Bertorini T, Graves MC, Mozaffar T, Jackson CE, Bosch P, McVey A, Dick A, Barohn R, Lomen-Hoerth C, Rosenfeld J, O'connor DT, Zhang K, Crook R, Ryberg H, Hutton M, Katz J, Simpson EP, Mitsumoto H, Bowser R, Miller RG, Appel SH, Stephan DAN. Whole-genome analysis of sporadic amyotrophic lateral sclerosis. *Engl J Med.* 2007; 357(8):775-88.

Fagerberg L, Hallström BM, Oksvold P, Kampf C, Djureinovic D, Odeberg J, Habuka M, Tahmasebpoor S, Danielsson A, Edlund K, Asplund A, Sjöstedt E, Lundberg E, Szigyarto CA, Skogs M, Takanen JO, Berling H, Tegel H, Mulder J, Nilsson P, Schwenk JM, Lindskog C, Danielsson F, Mardinoglu A, Sivertsson A, von Feilitzen K, Forsberg M, Zwahlen M, Olsson I, Navani S, Huss M, Nielsen J, Ponten F, Uhlén M. Analysis of the human tissue-specific expression by genome-wide integration of transcriptomics and antibody-based proteomics. Mol Cell Proteomics. 2014 Feb;13(2):397-406. doi: 10.1074/mcp.M113.035600. Epub 2013 Dec 5. PMID: 24309898; PMCID: PMC3916642.

Furlow D, Watson M, Waddell D, Neff E, Baehr L, Ross A, Bodine S. Altered gene expression patterns in muscle ring finger 1 null mice during denervation- and dexamethasone-induced muscle atrophy. *Physiological Genomics.* 2013;45(23):1168-1185. doi: 10.1152/physiolgenomics.00022.2013

Futterman S, Roe JH. The identification of ribulose and L-xylulose in human and rat urine. J Biol Chem. 1955 Jul;215(1):257-62. PMID: 14392159.

Ge T, Yang J, Zhou S, Wang Y, Li Y, Tong X. The Role of the Pentose Phosphate Pathway in Diabetes and Cancer. Front Endocrinol (Lausanne). 2020 Jun 9;11:365. doi: 10.3389/fendo.2020.00365. PMID: 32582032; PMCID: PMC7296058.

Hayes CS, Labuzan SA, Menke JA, Haddock AN, Waddell DS. Ttc39c is upregulated during skeletal muscle atrophy and modulates ERK1/2 MAP kinase and hedgehog signaling. J Cell Physiol. 2019 Dec;234(12):23807-23824. doi: 10.1002/jcp.28950. Epub 2019 Jun 12. PMID: 31188487.

Heinrich PC, Morris HP, Weber G. Behavior of transaldolase (EC 2.2.1.2) and transketolase (EC 2.2.1.1) Activities in normal, neoplastic, differentiating, and regenerating liver. Cancer Res. 1976 Sep;36(9 pt.1):3189-97. PMID: 10080.

Hitachi K, Tsuchida K. Role of microRNAs in skeletal muscle hypertrophy. *Front Physiol*. 2014;4:408. Published 2014 Jan 16. doi:10.3389/fphys.2013.00408

Hurley JH. The sugar kinase/heat shock protein 70/actin superfamily: implications of conserved structure for mechanism. Annu Rev Biophys Biomol Struct. 1996;25:137-62. doi: 10.1146/annurev.bb.25.060196.001033. PMID: 8800467.

Hurley JH, Faber HR, Worthylake D, Meadow ND, Roseman S, Pettigrew DW, Remington SJ. Structure of the regulatory complex of Escherichia coli IIIGlc with glycerol kinase. *Science*. 1993;259(5095):673-7. PMID: 8430315.

Ikeda, K., Inoue, S. TRIM PROTEINS AS RING FINGER E3 UBIQUITIN LIGASES. In: Madame Curie Bioscience Database [Internet]. Austin (TX): Landes Bioscience; 2000-2013.

Jin J, Li X, Gygi SP, Harper JW. Dual E1 activation systems for ubiquitin differentially regulate E2 enzyme charging. Nature. 2007 Jun 28;447(7148):1135-8. doi: 10.1038/nature05902. PMID: 17597759.

Labuzan SA, Lynch SA, Cooper LM, Waddell DS. Inhibition of protein phosphatase methylesterase 1 dysregulates MAP kinase signaling and attenuates muscle cell differentiation. Gene. 2020 May 20;739:144515. doi: 10.1016/j.gene.2020.144515. Epub 2020 Feb 26. PMID: 32112987.

Lang F, Aravamudhan S, Nolte H, Türk C, Hölper S, Müller S, Günther S, Blaauw B, Braun T, Krüger M. Dynamic changes in the mouse skeletal muscle proteome during denervation-induced atrophy. Dis Model Mech. 2017 Jul 1;10(7):881-896. doi: 10.1242/dmm.028910. Epub 2017 May 25. PMID: 28546288; PMCID: PMC5536905.

Lynch SA, McLeod MA, Orsech HC, Cirelli AM, Waddell DS. Zinc finger protein 593 is upregulated during skeletal muscle atrophy and modulates muscle cell differentiation. Exp Cell Res. 2019 Oct 15;383(2):111563. doi: 10.1016/j.yexcr.2019.111563. Epub 2019 Aug 20. PMID: 31442450.

MacAulay K, Woodgett JR. Targeting glycogen synthase kinase-3 (GSK-3) in the treatment of Type 2 diabetes. Expert Opin Ther Targets. 2008 Oct;12(10):1265-74. doi: 10.1517/14728222.12.10.1265. PMID: 18781825; PMCID: PMC4485462.

Madeira F, Park YM, Lee J, Buso N, Gur T, Madhusoodanan N, Basutkar P, Tivey ARN, Potter SC, Finn RD, Lopez R. The EMBL-EBI search and sequence analysis tools APIs in 2019. *Nucleic Acids Research.* 2019;47(W1):W636-W641. doi: 10.1093/nar/gkz268.

Mearini G, Schlossarek S, Willis MS, Carrier L. 2008. The ubiquitin-proteasome system in cardiac dysfunction. Biochim Biophys Acta, 1782: 749-763

McCroskery S, Thomas M, Maxwell L, Sharma M, Kambadur R. 2003. Myostatin negatively regulates satellite cell activation and self-renewal. J Cell Biol 162:1135–1147

Medina R, Wing S, Goldberg AL. Increase in levels of polyubiquitin and proteasome mRNA in skeletal muscle during starvation and denervation atrophy. Biochem J. 1995;307:631–637.

Moresi V, Williams AH, Meadows E, Flynn JM, Potthoff MJ, McAnally J, Shelton JM, Backs J, Klein WH, Richardson JA, Bassel-Duby R, Olson EN. Myogenin and class II HDACs control neurogenic muscle atrophy by inducing E3 ubiquitin ligases. Cell. 2010 Oct 1;143(1):35-45. doi: 10.1016/j.cell.2010.09.004. PMID: 20887891; PMCID: PMC2982779.

Omelchenko MV, Galperin MY, Wolf YI, Koonin EV. Non-homologous isofunctional enzymes: a systematic analysis of alternative solutions in enzyme evolution. *Biol Direct*. 2010; 5: 31.

Ormö M, Bystrom CE, Remington SJ. Crystal structure of a complex of Escherichia coli glycerol kinase and an allosteric effector fructose 1,6-bisphosphate. *Biochemistry.* 1998;37(47):16565-16572. DOI: 10.1021/bi981616s.

Penna F, Costamagna D, Fanzani A, Bonelli G, Baccino FM, and Costelli P. Muscle wasting and impaired Myogenesis in tumor bearing mice are prevented by ERK inhibition. 2010. *PLoS One* 5:e13604. doi: 10.1371/journal.pone.0013604

Sandri M, Sandri C, Gilbert A, Skurk C, Calabria E, Picard A, Walsh K, Schiaffino S, Lecker SH, Goldberg AL. Foxo transcription factors induce the atrophy-related ubiquitin ligase atrogin-1 and cause skeletal muscle atrophy. Cell. 2004 Apr 30;117(3):399-412. doi: 10.1016/s0092-8674(04)00400-3. PMID: 15109499; PMCID: PMC3619734.

Shi H, Scheffler J, Zeng C, Pleitner J, Hannon K, Grant A, Gerrard D. Mitogen-activated protein kinase signaling is necessary for the maintenance of skeletal muscle mass. *Am J Physiol Cell Physiol.* 2009;296(5):C1040-C1048. doi: 10.1152/ajpcell.00475.2008

Singh C, Glaab E, Linster CL. Molecular Identification of d-Ribulokinase in Budding Yeast and Mammals. *J Biol Chem*. 2017;292(3):1005–1028. doi:10.1074/jbc.M116.760744.

Stanford KI, Middelbeek RJ, Townsend KL, Lee MY, Takahashi H, So K, Hitchcox KM, Markan KR, Hellbach K, Hirshman MF, Tseng YH, Goodyear LJ. A novel role for subcutaneous adipose tissue in exercise-induced improvements in glucose homeostasis. Diabetes. 2015 Jun;64(6):2002-14. doi: 10.2337/db14-0704. Epub 2015 Jan 20. PMID: 25605808; PMCID: PMC4439563.

Stewart MD, Ritterhoff T, Klevit RE, Brzovic PS. E2 enzymes: more than just middle men. Cell Res. 2016;26(4):423-440. doi:10.1038/cr.2016.35

Stouth DW, vanLieshout TL, Ng SY, Webb EK, Manta A, Moll Z, Ljubicic V. CARM1 Regulates AMPK Signaling in Skeletal Muscle. iScience. 2020 Nov 2;23(11):101755. doi: 10.1016/j.isci.2020.101755. PMID: 33241200; PMCID: PMC7672286.

Sun Y, Bao Q, Xuan B, Xu W, Pan D, Li Q, Qian Z. Human Cytomegalovirus Protein pUL38 Prevents Premature Cell Death by Binding to Ubiquitin-Specific Protease 24 and Regulating Iron Metabolism. J Virol. 2018 Jun 13;92(13):e00191-18. doi: 10.1128/JVI.00191-18. PMID: 29695420; PMCID: PMC6002719.

Taillandier D, Aurousseau E, Meynial-Denis D, Bechet D, Ferrara M, Cottin P, et al. Coordinate activation of lysosomal, Ca 2+-activated and ATP-ubiquitin-dependent proteinases in the unweighted rat soleus muscle. Biochem J. 1996;316:65–72.

Taylor JA, Shioda K, Mitsunaga S, Yawata S, Angle BM, Nagel SC, Vom Saal FS, Shioda T. Prenatal Exposure to Bisphenol A Disrupts Naturally Occurring Bimodal DNA Methylation at Proximal Promoter of fggy, an Obesity-Relevant Gene Encoding a Carbohydrate Kinase, in Gonadal White Adipose Tissues of CD-1 Mice. *Endocrinology*. 2018; 159(2): 779–794.

Temparis S, Asensi M, Taillandier D, Aurousseau E, Larbaud D, Obled A, et al. Increased ATP-ubiquitin-dependent proteolysis in skeletal muscles of tumor-bearing rats. Cancer Res. 1994;54:5568–5573.

Tsai S, Sitzmann JM, Dastidar SG, et al. Muscle-specific 4E-BP1 signaling activation improves metabolic parameters during aging and obesity. *J Clin Invest*. 2015;125(8):2952-2964. doi:10.1172/JCI77361

Vendeville A, Winzer K, Heurlier K, Tang CM, Hardie KR. Making 'sense' of metabolism: autoinducer-2, LuxS and pathogenic bacteria. *Nat Rev Microbiol*. 2005 May;3(5):383-96. doi: 10.1038/nrmicro1146. PMID: 15864263.

Wagner KR, Kauffman FC, Max SR. The pentose phosphate pathway in regenerating skeletal muscle. The Biochemical Journal. 1978 Jan;170(1):17-22. DOI: 10.1042/bj1700017.

Wang L, Hashimoto Y, Tsao CY, Valdes JJ, Bentley WE. Cyclic AMP (cAMP) and cAMP receptor protein influence both synthesis and uptake of extracellular autoinducer 2 in Escherichia coli. J Bacteriol. 2005 Mar;187(6):2066-76. doi: 10.1128/JB.187.6.2066-2076.2005. PMID: 15743955; PMCID: PMC1064054.

Wing SS. Deubiquitinases in skeletal muscle atrophy. Int J Biochem Cell Biol. 2013 Oct;45(10):2130-5. doi: 10.1016/j.biocel.2013.05.002. Epub 2013 May 13. PMID: 23680672; PMCID: PMC5734930.

Xavier KB, Millern ST, Lu W, Kim JH, Rabinowitz J, Pelczer I, Semmelhack MF, Bassler BL. Phosphorylation and processing of the quorum-sensing molecule autoinducer-2 in enteric bacteria. *ACS Chemical Biology*. 2007 Feb;2(2):128-136. DOI: 10.1021/cb600444h.

Zhao J, Brault JJ, Schild A, Cao P, Sandri M, Schiaffino S, Lecker SH, Goldberg AL. FoxO3 coordinately activates protein degradation by the autophagic/lysosomal and proteasomal pathways in atrophying muscle cells. Cell Metab. 2007; 6: 472-483.

Zhang J, Liu F. Tissue-specific insulin signaling in the regulation of metabolism and aging. IUBMB Life. 2014 Jul;66(7):485-95. doi: 10.1002/iub.1293. Epub 2014 Aug 4. PMID: 25087968; PMCID: PMC4140976.

Zhang L, Nemzow L, Chen H, Lubin A, Rong X, Sun Z, Harris TK, Gong F. The deubiquitinating enzyme USP24 is a regulator of the UV damage response. Cell Rep. 2015 Jan 13;10(2):140-7. doi: 10.1016/j.celrep.2014.12.024. Epub 2015 Jan 8. PMID: 25578727; PMCID: PMC4359050.

Zhang R, Zhang F, Sun Z, Liu P, Zhang X, Ye Y, Cai B, Walsh M, Ren X, Hao X, Zhang W, Yu J. LINE-1 Retrotransposition Promotes the Development and Progression of Lung Squamous Cell Carcinoma by Disrupting the Tumor-Suppressor Gene FGGY. *Cancer Res* September 1 2019; 79(17): 4453-4465; DOI: 10.1158/0008-5472.CAN-19-0076

Zhang Y, Zagnitko O, Rodionova I, Osterman A, Godzik A. The FGGY carbohydrate kinase family: insights into the evolution of functional specificities. *PLoS Comput Biol*. 2011;7(12):e1002318. doi:10.1371/journal.pcbi.1002318

Zhu P, Zhou W, Wang J, Puc J, Ohgi KA, Erdjument-Bromage H, Tempst P, Glass CK, Rosenfeld MG. A histone H2A deubiquitinase complex coordinating histone acetylation and H1 dissociation in transcriptional regulation. Mol Cell. 2007 Aug 17;27(4):609-21. doi: 10.1016/j.molcel.2007.07.024. PMID: 17707232; PMCID: PMC2709280.

Zhu S, Tian Z, Torigoe D, Zhao J, Xie P, Sugizaki T, Sato M, Horiguchi H, Terada K, Kadomatsu T, Miyata K, Oike Y. Aging- and obesity-related peri-muscular adipose tissue accelerates muscle atrophy. PLoS One. 2019 Aug 23;14(8):e0221366. doi: 10.1371/journal.pone.0221366. PMID: 31442231; PMCID: PMC6707561.

ANASTASIA SMITH

EDUCATION

MS University of North Florida, Biology December 2020
Thesis: Fggy Carbohydrate Kinase Domain Containing (Fggy) is Induced During Skeletal Muscle Atrophy and Modulates MAP Kinase and AKT Signaling
Advisor: David Waddell

BA University of North Florida, Education December 2017
Secondary Biology

RESEARCH EXPERIENCE

The Mayo Clinic, Jacksonville, FL to begin December 2020
Special Project Associate II
Principal Investigator: Dr. LaTonya J. Hickson, Nephrology and Hypertension

University of North Florida, Jacksonville, FL 2018 to 2020
Graduate Student
Advisor: Dr. David Waddell

University of North Florida, Jacksonville, FL 2017
Advisor: Dr. Brian Zoellner

LABORATORY SKILLS

- Cell culture: C_2C_{12} mouse myoblast, 3T3, and HEK293T cell lines, maintain colony, plate experiments, treat cells
- Protein Analysis and Manipulation: Isolation, Western blot, cell fractionation, coimmunoprecipitation, confocal microscopy, site directed mutagenesis, protein overexpression, biochemical assays
- Genetic Analysis and Manipulation: Isolation, molecular cloning, qPCR, PCR,
- General management, maintenance, and usage of laboratory equipment, measurement methods, and practice of sterile techniques

TEACHING EXPERIENCE

University of North Florida, Jacksonville, FL August 2019 to December 2020
Graduate Teaching Assistant

- Lab instructor for General Biology I

Mandarin Oaks Elementary School, Jacksonville, FL June 2020 to July 2020
STEM Coordinator of Summer Camp

- Design experiments exploring STEM topics for students

Biology Teacher
Fletcher High School, Jacksonville, FL January 2018 to June 2018

- Taught Biology, Anatomy, and Marine Science